Nano-hydroxyapatite and bone derived extracellular matrix biomimetic composite coating on 316L stainless steel

A thesis submitted in partial fulfillment of the requirements for the degree of

Master of Technology in Biotechnology

By

RIK DHAR

213BM2021

Under the supervision of

DR. AMIT BISWAS
and
DR. SIRSENDU SEKHAR RAY

Department of Biotechnology & Medical Engineering

National Institute of Technology Rourkela-769008, Orissa, India

2015

Department of Biotechnology & Medical Engineering
National Institute of Technology, Rourkela, Orissa, India

Certificate

This is to certify that the thesis entitled "**Nano-hydroxyapatite and bone derived extracellular matrix biomimetic composite coating on 316L stainless steel**" by Mr. Rik Dhar, submitted to the National Institute of Technology, Rourkela for the Degree of Master of Technology is a record of bonafide research work, carried out by him in the Department of Biotechnology and Medical Engineering under my supervision and guidance. To the best of my knowledge, the matter embodied in this thesis has not been submitted to any other University/ Institute for the award of any Degree or Diploma.

Dr. Sirsendu Sekhar Ray
Assistant Professor
Department of Biotechnology and Medical Engineering
National Institute of Technology, Rourkela

Dr. Amit Biswas
Assistant Professor
Department of Biotechnology and Medical Engineering
National Institute of Technology, Rourkela

ACKNOWLEDGEMENT

This project would not have been possible without the help, support and guidance of so many people. Without the acknowledgement and appreciation of those, this project will remain incomplete. I would like to express my gratitude and regards from my heart to my supervisors **Dr. Amit Biswas** and **Dr. Sirsendu Sekhar Ray**, Department of Biotechnology and Medical Engineering for giving me an opportunity to do this project work and keeping faith on me for carrying out my work.

I am grateful to **Department of Ceramic Engineering**, the **Department Metallurgical and Materials Engineering**, the **Department of Physics** and **Department of Life Science** for allowing me to use their facilities and infrastructure. I would like to thank **Dr. Krishna Pramanik**, Department of Biotechnology and Medical Engineering, National Institute of Technology Rourkela for the support and opportunity she provided for this project.

Further, I would like convey my heartfelt gratititude to **Miss Saheli Saha, Miss Priyanka Goyal, Mr. Joseph Christakiran, Mr. Narendra Babu** and **Miss Abinaya** for their help and advice throughout my project work. I also sincerely thank my faculty members.

Finally, I am grateful to my parents **Col. Bappaditya Dhar** and **Dr. Sanchita Dhar**, family and friends for their love and support, which kept me motivated throughout this project. Above all, I am grateful to **God**.

CONTENTS

Abstract v
List of Figures vi
List of tables vii
1 Introduction 1
2 Literature Survey 3
2.1 HAP synthesis 3
2.2 Various deposition methods of HAP on 316L stainless steel 4
2.3 Demineralized bone matrix and Bone ECM 8
3 Materials and Methods 9
3.1 Fabrication of various devices 9
3.1.1 Sample polishing device 9
3.1.2 Electrophoretic deposition setup 10
3.1.3 Dip-coating device 13
3.2 Preparation of 316L Stainless Steel samples 14
3.2.1 Grinding and polishing 14
3.2.2 Chemical treatment 14
3.3 nano-Hydroxyapatite synthesis 15
3.3.1 Wet chemical method synthesis 15
3.3.2 Characterizations 17
3.4 Electrophoretic deposition of nano-Hydroxyapatite 18
3.4.1 Methods and optimization of process 18
3.4.2 Sintering 18
3.4.3 Characterizations 19
3.5 Bovine bone Extracellular Matrix extraction 20
3.5.1 Extraction and de-cellularization 20
3.5.2 Characterization 21
3.6 preparation of nano-hydroxyapatite- bECM composite 22
3.6.1 Wet chemical method 22
3.6.2 Characterization 23
3.7 Dip coating of bECM and nano-hydroxyapatite-bECM composite 24

3.8 In vitro cell proliferation assays 25
4 Results and Discussions 26
4.1 Synthesized nano-Hydroxyapatite characterization and electrophoretic Deposition studies 26
4.1.1 Study of samples prepared by electrophoretic deposition 26
4.1.2 Kinetic study of electrophoretic deposition 27
4.1.3 Modified electrophoretic deposition procedure to reduce crack formation 28
4.1.4 Particle size analysis 28
4.1.5 DSC-TG of nano-hydroxyapatite 29
4.1.6 XRD of nano-hydroxyapatite before and after sintering 30
4.1.7 FTIR 33
4.1.8 FE-SEM analysis 34
4.2 Bone derived ECM (bECM) characterization and analysis 35
4.2.1 Protein estimation using Lowry's Method 35
4.2.2 Collagen Estimation 35
4.2.3 SDS PAGE 36
4.3 nHAP-bECM composite 37
4.3.1 FTIR of samples in solution form 37
4.3.2 Crystallinity of samples using XRD and FTIR 38
4.3.3 DSC-TGA 40
4.3.4 FE-SEM 41
4.4 In-vitro Cell proliferation and differentiation assay 42
4.5 Conclusion 43
References 44

ABSTRACT

In this project 316L stainless steel samples were polished, chemical treated and were coated with synthesized nano hydroxyapatite by modified electrophoretic deposition method consisting of coating the same sample multiple times to reduce cracks. Extracellular matrix from bovine bone was extracted and was used to synthesize biomimetic nano-hydroxyapatite and bone derive extracellular matrix composites. These were then used to coat the steel samples on top of the base nano hydroxyapatite coating. The base coat, the bone derived extracellular matrix and the nano-hydroxyapatite and bone derive extracellular matrix composites were characterized. The synthesized nano-hydroxyapatite were found to be nano rod in shape. The extracellular matrix had an 82% collagen content as well as other essential non-collagen proteins. The composites showed a significant higher cell proliferation than the hydroxyapatite.

LIST OF FIGURES

Figure 3.1: Schematics of polishing device 9
Figure 3.2 Polishing apparatus 10
Figure 3.3: Electrophoretic deposition setup; a) cathode part kept on the weighing balance plate; b) anode part; c) anode and cathode part together; d) the sample and graphite rod; and e) the complete setup inside the weighing balance 11
Figure 3.4: Schematics of electrophoretic deposition setup 12
Figure 3.5: RsCom Ver. 4.01 software used to record the data from the weighing balance 12
Figure 3.6: Schematics of dip coating device 13
Figure 3.7: Sample after grinding (right) 14
Figure 3.8: Hydroxyapatite synthesis: wet chemical method 16
Figure 3.9: Dip coating of sample using the dip coating device 24
Figure 4.1: Picture of samples after EPD of nano-hydroxyapatite at 100V, a) 5g/l, b) 10g/l, c) 20g/l; and 200V, d) 5g/l, e) 10g/l, f) 20g/l 26
Figure 4.2: SEM images of sample 5g/l deposited at a) 100V and b) 200V 26
Figure 4.3: Deposition kinetics during EPD at 100V and 200V 27
Figure 4.4: Deposited nano-hydroxyapatite after a) first coat, b) after drying and c) after second coat 28
Figure 4.5: Size distribution curve of nano-hydroxyapatite 28
Figure 4.6: DSC-TG study of nano-hydroxyapatite powder deposited over 316L stainless steel samples 29
Figure 4.7: XRD of nano-hydroxyapatite a) before and b) after sintering 30
Figure 4.8: FTIR of nano-hydroxyapatite a) before and b) after sintering 33
Figure 4.9: FE-SEM of samples a) before and b) after sintering at 900°C 34
Figure 4.10: FE-SEM of deposited nano-hydroxyapatite at 30V interval EPD showing a) micro crack and its b) magnification 34
Figure 4.11: Lowry's protein estimation standard curve 35
Figure 4.12: SDS PAGE of bovine derive extracellular matrix 36
Figure 4.13 FTIR of sample in solution form 37
Figure 4.14: XRD of nano-hydroxyapatite-bECM composite samples (S2-S5) and HAP as control (S1) 39
Figure 4.15: FTIR of nano-hydroxyapatite-bECM composite samples (S2-S5) and HAP as control (S1) 39
Figure 4.16: DSC of nano-hydroxyapatite-bECM composite samples (S2-S5) and HAP as control (S1) 40
Figure 4.17: TGA of nano-hydroxyapatite-bECM composite samples (S2-S5) and HAP as control (S1) 40
Figure 4.18: FESEM of samples a) S1 (HAP), b) S2 (HAP + 0.5 bECM), c) S3 (HAP + 1.0 bECM), d) S4 (HAP + 1.5 bECM), e) S5 (HAP + 2.0 bECM), f) bECM 41
Figure 4.19: MTT cell proliferation assay of samples 42

LIST OF TABLES

Table 2.1: List of various techniques to deposit hydroxyapatite of metal surfaces.....4
Table 4.1: Crystalline size of selected planes of nano-hydroxyapatite before sintering 31
Table 4.2: Crystalline size of selected planes of nano-hydroxyapatite after sintering 31
Table 4.3 Crystallinity index of nano-hydroxyapatite-bECM composite samples.....38

1 INTRODUCTION

Stainless steel has been used extensively as a biomaterial for implants for many decades now. It is popular as an implant due to its properties such as corrosion resistivity, high mechanical strength and low cost when compared to other popular metal implant material like titanium and its various alloys [1]. Stainless steel is majorly used for short duration implants like bone pins and metal plates, that needs to be removed when bone wound healing and regeneration has occurred. Its use as a long term medical implant is limited as even though it is comparatively corrosion resistant, it is known to cause toxicity inside the body due to release of nickel and chromium ions in the physiological environment. [2] These ions can cause serious problems such as sarcomas, carcinogenicity, osteolysis, fibrous encapsulations. [3] Addition to these problems stainless steel implants do not show bioactivity and thus do not cause enough osteointegration which can lead to other problems such as loosening of implants leading to implant failure.

Literature have shown that surface modification of austenitic stainless steel can counteract many of these problems by decreasing ion leaching effects, increasing bioactivity and biocompatibility, while keeping the other essential properties of the implants intact. [4] Hydroxyapatite (HAP) ($Ca_{10}(PO_4)_6(OH)_2$) is very similar to mineral component of bone with its calcium to phosphate ratio almost equal to that of natural bone. Hydroxyapatite coating for metal implants have become very popular from its first report in the 1980s. Many research has been going on since then on coating of hydroxyapatite on metal surfaces and many techniques have been established. Hydroxyapatite coating on metal surfaces involves methods like plasma spraying, ion implant, laser surface modification, dip coating, electrophoretic deposition, sol-gel coating and invitro growing of hydroxyapatite on the metal surface. [5] [6] [7] [8]

Electrophoretic deposition is a low cost and effective method of surface coating through which complex shape objects can be coated with high purity substances, which is not easily possible with other methods. [9] Electrophoretic deposition of hydroxyapatite is a simple technique compared to others through which a layer of hydroxyapatite can be deposited with thickness ranging from micrometer to millimeter range depending on the parameters of the deposition technique. Parameters such as size of particles, type of ions, conductivity of the particle and the electrolyte, pH, etc. and the electrodes used in the electrophoretic deposition determines the quality of coating on the metal surface. [10]

The bioactivity and the osteointegration of a steel sample coated with hydroxyapatite can be further increased with use of biomimetic coating. Extracellular matrix has been used as biological scaffolds before. [11] As well as demineralized bone matrix has been used as bone graft for many decades [12]. Demineralized bone matrix contains mainly contains type I collagen and many other non-collagenous proteins and growth factors. [13] Objective of this study is to apply extensive decellularization method to xenogenic demineralized bone matrix and the use the resulting extracellular matrix to form a biomimetic composite of hydroxyapatite that can be coated on to 316L stainless steel. The composite coating containing collagen and other bone proteins should increase bioactivity of nano hydroxyapatite and the coated steel sample when used as implant should increase the osteointegration as well as the highly crystaline nano-hydroxyapatite base coating should avoid exposure of the steel to surround physiological environment preventing the problems related to steel medical implants that are mentioned above.

2 LITERATURE SURVEY

2.1 HAP SYNTHESIS

There are various methods that hydroxyapatite crystals can be prepared. One is wet chemical precipitation method. [14] The crystal shape, its size, surface area of the nano hydroxyapatite are very sensitive to the reaction parameters such as temperature of the reaction, pH of the solution etc. One way to obtain particle size less than a 100 nm is to stir the solution for 24 hours at room temperature. [15] Another method to synthesize is through simulated body fluid. A biomimetic hydroxyapatite is obtained from the salts present in the simulated body fluid solution at 37°C that can be deposited directly on a surface. [16] This hydroxyapatite is very similar to that of bone apatite and is carbonated similar to it. [17] Sol gel method is a low temperature method in which the Ca and P precursors are fused together through sintering. Various different types of precursors are used and are mixed in the ratio of 1.67 Ca to P and depending the precursor the shape and size of the crystals vary. [18]

2.2 VARIOUS DEPOSITION METHODS OF HAP ON 316L STAINLESS STEEL

Various methods have been reported in the literatures that have been listed in the table below

Table 2.1: List of various techniques to deposit hydroxyapatite of metal surfaces

Author and Journal	Material	Coater	Methods of Coating	Remarks
L. Pramatarova et al, Euroapean Cells and Materials Vol. 9. 2005 (pages 9-12)	AISI 316 Stainless Steel	ECM, Hap	The osteoblast-like cell line SAOS-2 was allowed to synthesize and assemble its own ECM on the substrates, 1st method: soaking in SBF; 2nd method: LLSI	Spherical aggregates of Hap of average 5µm diameter were observed
K. Prabakaran et al, Trends Biomater. Artif. Organs, Vol 19(2), pp 84-87 (2006)	316 L Stainless Steel	HAP powder synthesized by slow adition of H3PO4 to calcined eggshell solution	H3PO4 treatment for 1 hr, then electrophoretic deposition of HAP at 60V for 3min.	Use of eggshell for HAP preparation is cost effective. Cyclic polarization studies for long term in vitro corrosion.
Camila Molena de Assis et al, Materials Research, Vol. 8, No. 2, 207-211, 2005	Commercially pure Titanium	HAP	NoOH treated sample were immeresed in sodium silicate solution for 24hrs at 37C. Then immersed in 1.5 SBF at 37C for 6 days. Samples were heat treated at 400, 500, 600, 700, 800 C at rate of 5C/min	temp between 400 and 600 showed less crystallinity similar to biological HAP

Dongxia Liu et al, Surface & Coatings Technology 205 (2011) 3975–3986	316L Stainless Steel, Titanium, Aluminium , Copper	HAP	Electrochemical Deposition: Electrolyte solution consisiting of 1.67mM K2HPO4, 2.5mM CaCl2 & 138 mM NaCl in water, buffered to 7.2 using Tris-HCl. Metal used as cathod and platinum plate as anode placed in distance of 10mm, at 95C; Hydrothermal growth of HAP: .2 M Na2EDTA, .2 Ca(NO3)2 15 ml was mixed with .12M (NH4)2HPO4 15 ml adjusting pH to 10 with NH4OH. The sample were placed in pressure vessel for 15h at 200C	Various additional HAP crystal structure was studied at various hydrothermal temp of 160, 180, 220C and various pH of 8, 9, 11 and time of 5, 10, 60hrs. Surface integrity comparition was also done over EPD and hydrothermal deposition.
J. Gawronski et al, Archives of Foundry engineering Volume 9 Issue 3/2009 pp235-242	AISI 316L stainless steel	Carbon, HAP	120nm carbon layer deposition using Radio Frequency Plasma Assisted Chemical Vapour Deposition, HAP coating on it by Pulse Laser Deposition	
Dr.sami Abualnoun Ajee et al, Eng.&Tech.Vol.26,No.8,2008	316L Stainless Steel	HAP	Sample were soaked in 5N NaOH solution for 90C for 30min, then washed with Deionized water and dried. EPD for 1,2,3,4,5 at 60V	Aim of OCP-time measurement is to understand the corrosion behavior of the coated and uncoated specimens under equilibrated conditions

				in the simulated body environment.
L. Pramatarova et al, J Mater Sci: Mater Med (2007)	AISI 316 Stainless Steel	Ca and P ions	Ion implantion using High current Implanter at 104, 92, 80KeV for Ca and 61, 54, 47 KeV for P ions. Theoretical calculation for the process with Profile Code program, thermal treatment at 873K in air for 1hr.	formation of Ca and P-based compounds, such as HA, dicalcium phosphate dihydrate and octacalcium phosphate, CaO, CaCO3, Ca2P2O7, P2O5, as well as predominant oxides of Cr and Fe.
Vamsi Krishna Balla et al, Materials Science and Engineering C 33 (2013) 4594–4598	316 L Stainless Steel	Laboratory-synthesized crystalline HAP powder	Laser-engineered net shaping (LENS™), a commercial additive manufacturing process. Several coating samples, with 100 mm2 area, were prepared at a powder feed rate of 1.4 g/min with different laser powers and scan velocities.	SEM equipped with EDS. phases analysis using an X'Pert Pro MPD diffractometer. Vickers hardness measurements. biocompatibility evaluated by immersing them in SBF and studied for apatite precipitation.
Makoto Sasaki et al, Sci. Technol. Adv. Mater. 13 (2012) 064213 (8pp)	nickel-free high-nitrogen stainless steel (HNS)	Immobilized glutamic acid; Then CaP	TSC-i-HNS: HNS was pretreated with UV, then immersed in 20mM TSC/DMSO for 15 min, rinsed with DMSO and HFIP and dried in N2 gas, then immersed in HFIP for 15 min and vacuum dried for 12hrs. TSC-i-HNS was incubated with Glutamic acid at 4C for 3 hrs. Glu-	MG-63 adhesion and proliferation was less in HAp-coated HNS than in Org-HNS, but ALP activity was found to be more in HAp-coated HNS.

			i-HNS was immersed in 0.25M Ca-EDTA and 0.25M KH2PO4, pH8.1 Solution at 90C for 3, 6, 12, 2 hrs.	
Emilia Pecheva et al, Electrodeposition : Properties, Processes and Applications, chapter 11	AISI 316L stainless steel, commercial ly pure Ti	Nano diamond, HAP	ND particles were synthesized by the shock-wave propagation method through the detonation of trinitrotoluene and hexogen at high pressure and high temperature. Then purified. A ND-SBF suspension was prepared by ultrasonication for 20min as electrolyte. The deposition was performed in a three-electrode electrolytic cell. Then dried.	precoating with fibronectin (FN) even at low adsorption concentrations (1mg/ml) strongly improved cell adhesion and preferentially spreading on the HA-ND samples
L. Pramatarova et al, Euroapean Cells and Materials Vol. 9. 2005 (pages 9-12)	AISI 316 Stainless Steel	ECM, Hap	The osteoblast-like cell line SAOS-2 was allowed to synthesize and assemble its own ECM on the substrates, 1st method: soaking in SBF; 2nd method: LLSI	Spherical aggregates of Hap of average 5µm diameter were observed
K. Prabakaran et al, Trends Biomater. Artif. Organs, Vol	316 L Stainless Steel	HAP synthesize d by slow adition of H3PO4 to	H3PO4 treatment for 1 hr, then electrophoretic deposition of HAP at 60V for 3min.	Use of eggshell for HAP preparation is cost effective. Cyclic polarization studies for

19(2), pp 84-87 (2006)	calcined eggshell solution	long term in vitro corrosion.

2.3 DEMINERALIZED BONE MATRIX AND BONE ECM

Demineralized bone matrix products has been used clinically for a long time in a wide variety of applications in bone repair and regeneration comprising of 20% of total bone grafting procedures. It is acid extracted organic part of bone from various sources and is a commercially available as variety of products. It contains various proteins, some of which are unique to bone, growth factors, calcium and phosphate containing solids and minute amount of cell debris. When used in as bone grafts these materials in the demineralized bone matrix are slowly released into the wound area facilitating bone growth, integration and healing. Demineralized bone matrix has been known to show osteoinduction that is differentiation of mesenchymal stem cells into osteoblasts and osteoconduction that is growth of the bone tissue into the graft or implant. [19]

3 MATERIALS AND METHODS

3.1 FABRICATION OF VARIOUS DEVICES

At various stages of this project, different devices were fabricated to assist with the sample preparations.

3.1.1 Sample polishing device

316L Stainless steel samples were required to be polished with emery polishing papers after they had been grinded, to make the surface smooth and without defects. For this purpose a polishing device was fabricated to speed up the polishing step. Figure 3.1 shows the schematics of the polishing apparatus and Figure 3.2 shows the picture of the fabricated apparatus. The apparatus consists of two rolling drums. A strip of the emery paper is needed to be attached in a loop around these rolling drums. One of the rolling drums is driven by a 100 RPM geared motor. A platform is there in between the two rolling drums on which the emery polishing paper strips slides on. The steel sample is pressed down.

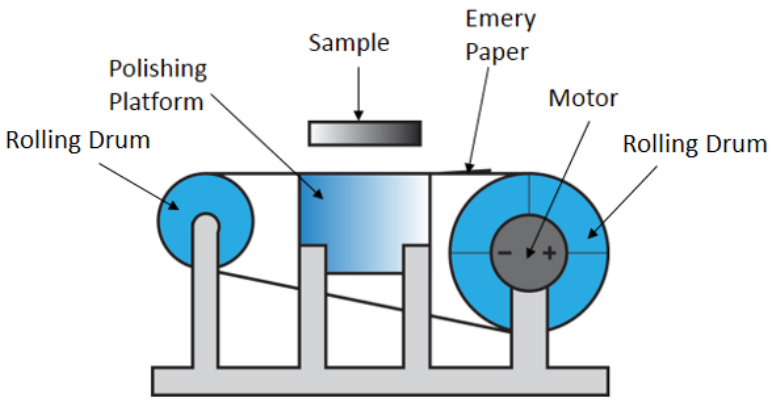

Figure 3.1: Schematics of polishing device

Figure 3.2 Polishing apparatus

3.1.2 Electrophoretic deposition setup

For deposition of nano-hydroxyapatite of 316L Stainless steel, electrophoretic deposition was carried out. For this purpose and to record the kinetics of deposition the following apparatus was setup as shown in Figure 3.3. The setup consists of cathode part in which consist of a two axis gimbal to which the steel sample was suspended from. The cathode part was free of the other parts of the setup and was kept on the weighing balance plate. The anode part consists of a platform to which a graphite rod attached, whose position can be adjusted with respect to the platform. The anode part was also free of the cathode part and was kept inside the weighing balance without disturbing the weighing balance plate. The cathode and anode was attached to a power supply using thin 0.2mm copper wires. The weighing balance was connected to a desktop computer using RS-232 9-pin serial cable. Data from the weighing balance was recorded using the software RsCom Ver. 4.01.

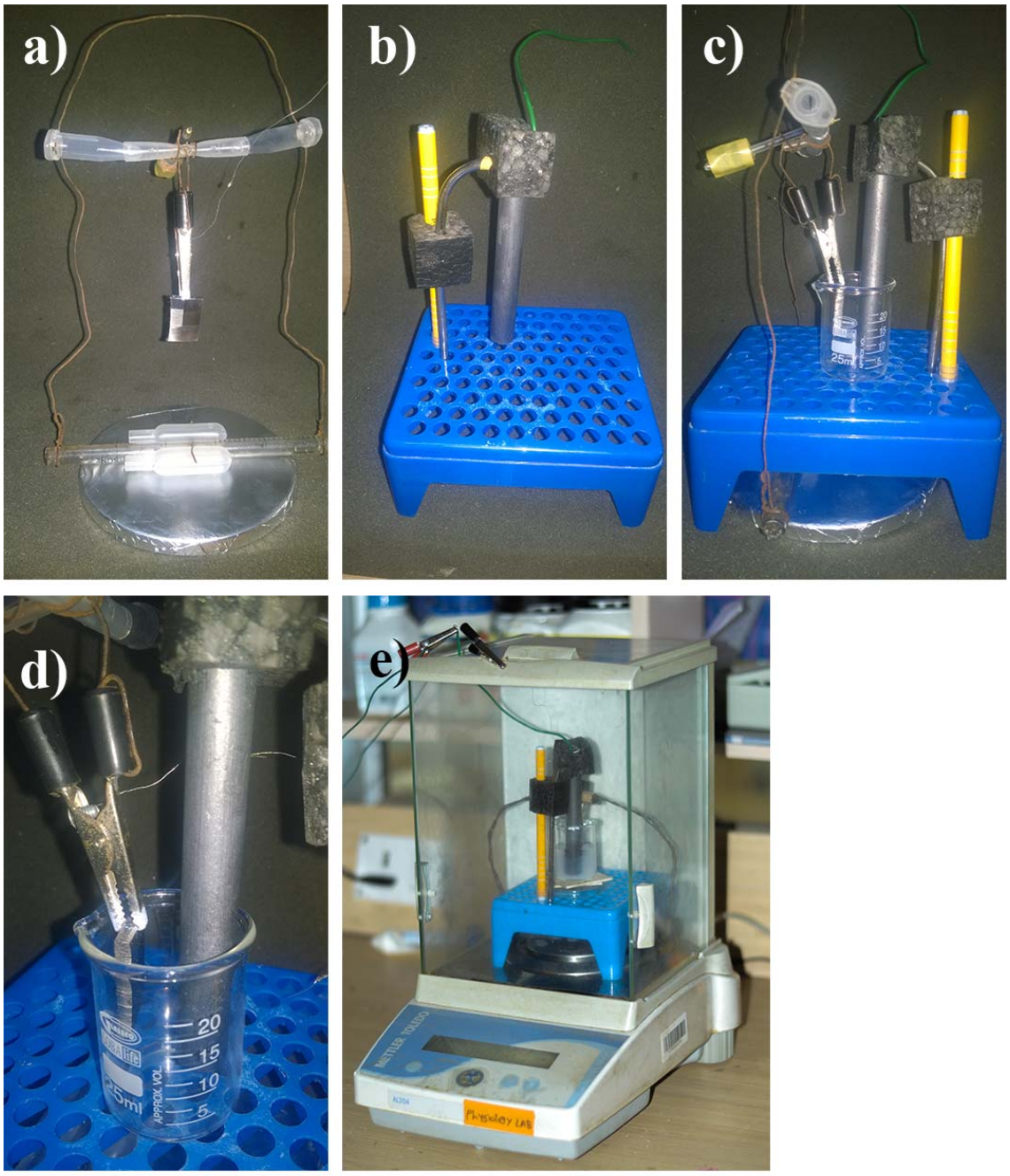

Figure 3.3: Electrophoretic deposition setup; a) cathode part kept on the weighing balance plate; b) anode part; c) anode and cathode part together; d) the sample and graphite rod; and e) the complete setup inside the weighing balance

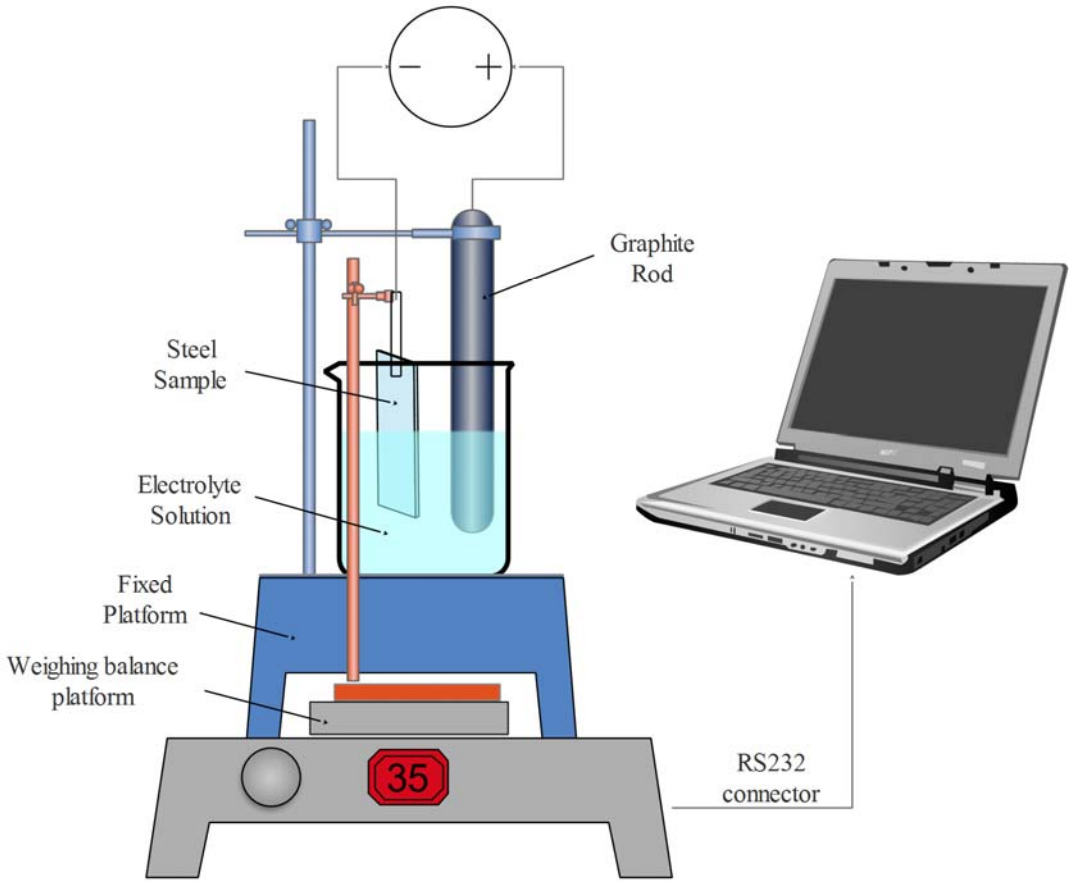

Figure 3.4: Schematics of electrophoretic deposition setup

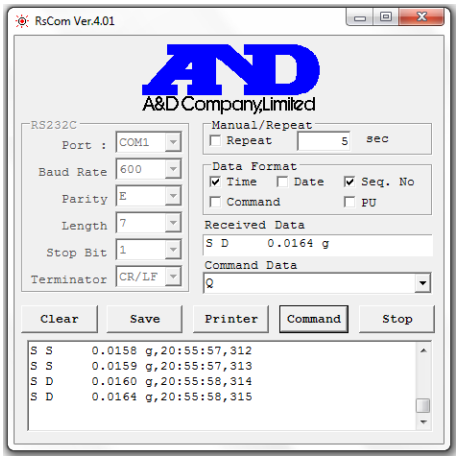

Figure 3.5: RsCom Ver. 4.01 software used to record the data from the weighing balance

3.1.3 Dip-coating device

For deposition of nanohydroxyapatite and bovine bone derived extracellular matrix composite, dip coating was used. A device was designed and fabricated to retract the samples from the solution at a very slow rate of 4mm per minute. Figure 3.6 shows the schematics of the device and Figure 3.7 shows the picture during dip coating. The device consisted of a fixed RPM motor (100RPM, 12V) and three disks. The motor drove an 11 mm diameter shank, which drove a 110mm diameter disk stepping down the rotation to 10RPM. This disk was then attached to an 11mm shank which drove another 110mm diameter disk, stepping the rotation further to 1RPM. This second disk then drove the third disk is similar way with the final rotational speed of the third disk being 0.1RPM. The third disk was attached to a 12.7mm diameter shank which coiled up a thread attached to it at a speed of 4mm per min. Sample was tied to this thread and was hanged over a smooth rod into the solution from which it was needed to be retracted.

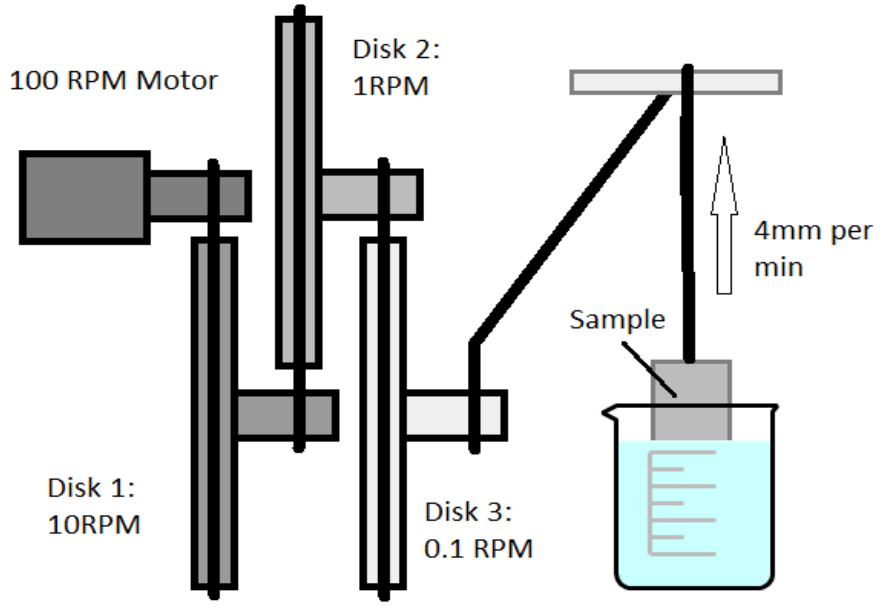

Figure 3.6: Schematics of dip coating device

3.2 PREPARATION OF 316L STAINLESS STEEL SAMPLES

3.2.1 Grinding and polishing

316L Stainless Steel samples of dimensions 25mm x 15 mm were sawed from a 4mm thick sheet. Then the samples were grinded to smoothen the sawed edges and round the sharp corners and sides. Using the fabricated polishing device the samples were polished with emery paper of size 1/0 and 2/0. Polishing with 3/0 and 4/0 emery paper was carried out manually to avoid the vibrations produced by the polishing machine. Steel samples were then washed with acetone and ethanol under ultrasonication to remove impurities.

Figure 3.7: Sample after grinding (right)

3.2.2 Chemical treatment

After polishing the samples were treated with chemicals to increase their hydrophilicity. The samples were kept in 1N NaOH solution for 6 hours at 50°C. Samples were then washed with deionized water using an ultrasonication. The samples were then dried and wrapped around soft dried tissue paper and were stored inside a vacuum desiccator.

3.3 NANO-HYDROXYAPATITE SYNTHESIS

3.3.1 Wet chemical method synthesis

Nano-hydroxyapatite was synthesized using wet chemical method. Figure 3.9 shows the setup for synthesis of hydroxyapatite. 0.05M calcium nitrate solution was prepared, heated to 80°C and its pH was adjusted to 10-11 range using ammonia solution. The calcium nitrate solution was then poured into a beaker over a hotplate magnetic stirrer. 0.03M di-hydrogen ammonium phosphate solution was also heated to 80°C and its pH was adjusted to 10-11 range using ammonium solution. This solution was then poured into a separator funnel and was kept over the calcium nitrate solution. The valve of the separator funnel was slowly opened to allow the ammonium phosphate solution to drop over the calcium nitrate. The temperature of the calcium nitrate solution was maintained at 80°C and was kept under vigorous stirring. The solution slowly turns milky white in color indicating the formation of hydroxyapatite. The resulting milky white solution was then cooled while being kept under constant stirring for another 24hrs at room temperature. After 24 hours the nano-hydroxyapatite precipitate is allowed to settle down in the beaker and the clear supernatant is removed carefully without disturbing the settled nanohydroxyapatite precipitates. The nano-hydroxyapatite slurry at the bottom is then centrifuged to form a pellet and the supernatant is removed. The pellet is then mixed with deionized water and ultrasonicated for 10 minutes and then again centrifuged. This step is repeated 3-4 times to wash the nano-hydroxyapatite particles and remove all impurities. Finally the pellets are removed into a petridish and is kept in an oven to dry at 90°C for 12 hours to get nano-hydroxyapatite powder.

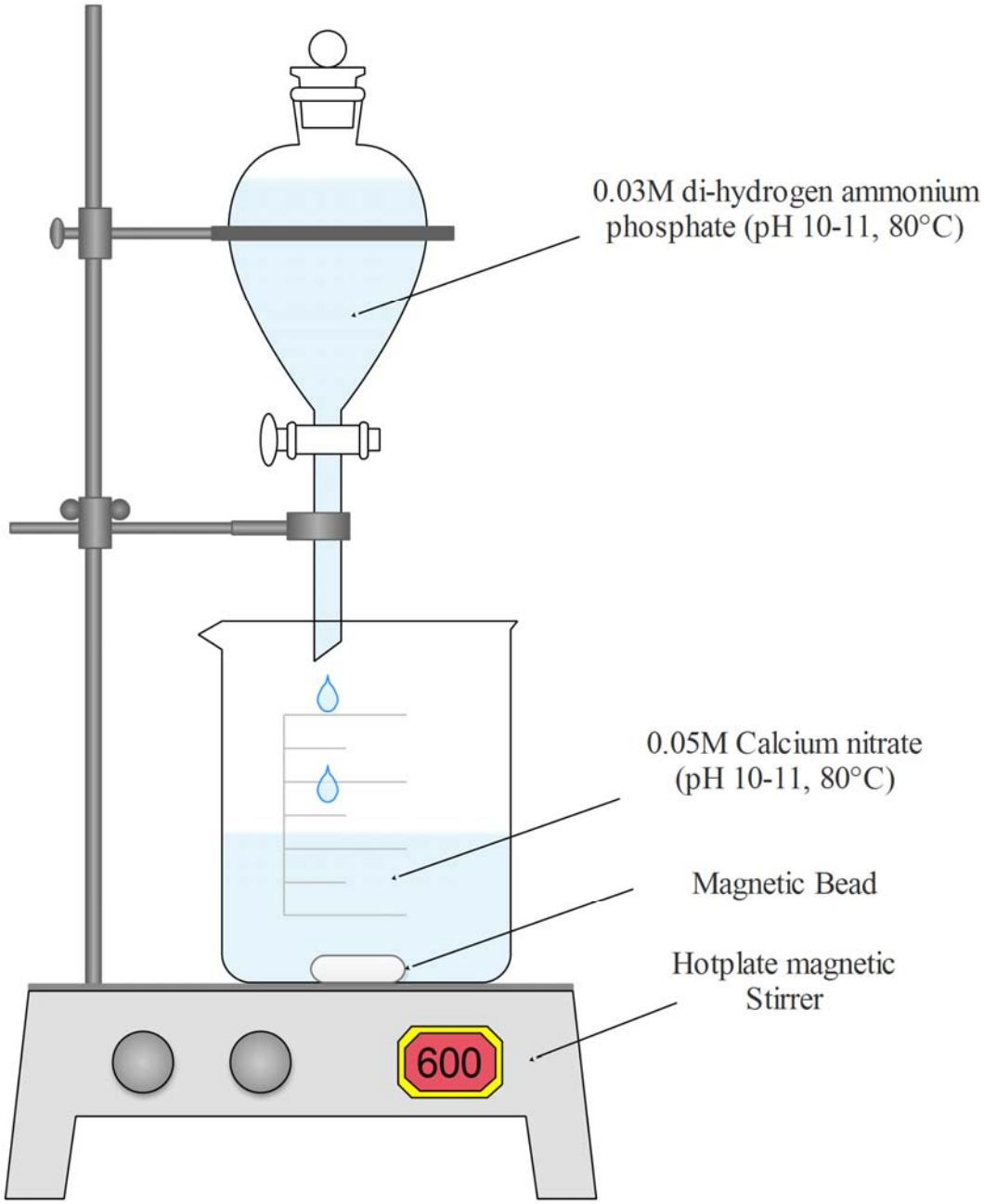

Figure 3.8: Hydroxyapatite synthesis: wet chemical method

3.3.2 Characterizations

Nano-hydroxyapatite powders were characterized by powder X-Ray diffraction using Ultima IV Multipurpose XRD Diffractometer (Rigaku Co., Tokyo, Japan). The instrument used an X-ray source of Cu-Kα, and was operated at a voltage of 40kV and a current of 40 mA. The analysis was done in the 2 θ range of 20° to 70° at a scan rate of 5°/min.

Fourier Transform Infrared spectroscopic study of the samples were done in order to analyze the chemical interactions and the bonds present in the sample. For the analysis, FTIR-spectrometer attached with an ATR cell of ZnSe was used (Alpha-E Bruker, Germany). The nano hydroxyapatite powders were analyzed in a wavenumber range of $4000cm^{-1}$-$500cm^{-1}$ at a resolution of $8cm^{-1}$ for a total of 25 scans.

Thermal measurements of the nano hydroxyapatite was carried using NETZSCH STA 449 C

Particle

3.4 ELECTROPHORETIC DEPOSITION OF NANO-HYDROXYAPATITE

3.4.1 Methods and optimization of process

To deposit nano-hydroxyapatite on the prepared stainless steel samples, electrophoretic deposition technique was used. For this purpose the electrophoretic deposition setup described in section 3.1.2 was used. Stainless steel samples were used as cathode and a graphite rod was used as anode. The distance between the two electrodes was kept as 10mm. Nano-hydroxyapatite was suspended in propanol at concentrations of 5g/L, 10g/L and 20g/L. These solution were then ultra-sonicated for 10 min and was used as the electrolyte solution in this electrophoretic deposition. A DC converter was used as the power source. Two voltages for each concentration of nano-hydroxyapatite in the electrolyte was used, i.e. 100V and 200V for 5 min each. Kinetic data of the deposition was recorded using a weighing balance connected to a computer using a RS232 connector cable and software called RsCom Ver. 4.01. The raw data was then converted to weight deposited per surface area and plotted against time.

The samples deposited by this method showed visible and microscopic cracks as seen in section 4.1. To reduce these crack formations on the surface of the samples, the electrophoretic deposition method was modified. Samples were deposited using a 10g/L concentration nano-hydroxyapatite propanol solution at 30V for 2 min. Then the sample was taken out of the solution and was allowed to dry in air at room temperature. Then the samples were again deposited with same parameter. These step was done a total of three times.

3.4.2 Sintering

Nano hydroxyapatite coated stainless steel samples were sintered using a tube furnace in Argon atmosphere. The temperature was raised to 900°C at a constant rate of 10°C/min. Then the samples were kept at 900°C for 2 hours holding. Then the furnace was allowed to be cooled down to room temperature overnight.

3.4.3 Characterizations

Nano-hydroxyapatite solutions were characterized by powder X-Ray diffraction and Fourier Transform Infrared spectroscopic study by the same way mentioned in section 3.3.2.

The morphology of the nHAP coated on the steel samples was analyzed using a Field Emission Scanning Electron Microscope (Nova Nano Sem, FEI). The samples were mounted onto the stubs and were gold coated for 4-5 min. using (QS 1050 Quorum Tech.) sputter coater. The samples were then loaded into the instrument and thus the micrographs were obtained at an accelerating voltage of 10-15 kV. The micrographs were obtained from different positions on the sample and thus at least five micrographs were obtained.

3.5 BOVINE BONE EXTRACELLULAR MATRIX EXTRACTION

3.5.1 Extraction and de-cellularization

To extract extracellular matrix from bone, previously reported protocol was followed. In brief, bovine femur was collected from licensed slaughter house. Cancellous part of the femur was separated from the rest of the bone by using a butcher's knife and a hammer. The cancellous bone were further chopped into small pieces. These small pieces were then grinded into a thick paste using a food processor. The resulting bone paste was then added into 0.5 N HCl solution kept for stirring for 48 hours using an overhead stirrer, for demineralization. Solution was changed every 12 hours by filtering the undissolved bone matrix out and discarding the supernatant. The resulting demineralized bone matrix was then washed repeatedly with deionized water. Then to remove lipids and fats the demineralized bone matrix was washed with 1:2 methanol-chloroform solution using a soxlate apparatus running 20 cycles till the extract solution from the bone matrix was clear. The demineralized bone matrix was then washed with methanol and then deionized water. For decellularization it was then kept in 0.05% trypsin-EDTA solution for 24 hours in a CO_2 incubator and then washed repeatedly with deionized water. Resulting demineralization and decellularization bone matrix was then digested using pepsin-HCL solution for another 96 hours. After that the pH of resulting viscous solution was neutralized and salts were removed by dialysis. The solution was then stored in -20°C. Part of the solution was lyophilized for characterizations.

3.5.2 Characterization

Protein content of the solution was estimated by Lowry's method. BSA was used to plot the standard curve and OD was taken at 660nm using a UV-Vis spectrophotometer. To determine the collagen content of the bECM hydroxyproline assay was done. Lyophilized samples were acid hydrolyzed at 120°C in 1N HCl. Hydroxyproline was used as reference to plot the standard curve. OD was taken at 550nm using a UV-Vis spectrophotometer.

SDS-PAGE was carried out for the extracted bECM sample by using the Laemmili's discontinuous buffer system in order to see the purity of the extracted sample as well as to see the presence of the bands corresponding to the proteins present in the sample. Biorad mini gel electrophoresis setup (see company name) was used according to the manufacturer's instructions. The electrophoresis was carried out using a resolving gel of 12% and a stacking gel of 5% at a constant voltage of 120 kV. The bands were viewed by staining with Coomassie Brilliant Blue R 250 (SRL Pvt. Ltd., Mumbai, India). Prior boiling of the samples were done in the loading buffer and 20 µl of it was added in the wells. A broad range marker having molecular weight range from 3.5 to 205 kDa was used.

3.6 PREPARATION OF NANO-HYDROXYAPATITE- BECM COMPOSITE

3.6.1 Wet chemical method

To prepare the nano-hydroxyapatite and bone derived extracellular matrix composite wet chemical method of hydroxyapatite was modified. 0.05M calcium nitrate solution was prepared, heated to 50°C and its pH was adjusted to 9-10 range using ammonia solution. The calcium nitrate solution was then poured into a beaker over a hotplate magnetic stirrer. To this solution bone derived extracellular matrix (bECM) was added at varying concentration. That is sample S1 had no bECM added to it and acted as control for comparison. Sample S2, S3, S4 and S5 had bECM added to it so that the final reaction solution concentration would have been 0.5g/l, 1g/l, 1.5g/l and 2g/l respectively. 0.03M di-hydrogen ammonium phosphate solution was also heated to 50°C and its pH was adjusted to 9-10 range using ammonium solution. This solution was then poured into a separator funnel and was kept over the calcium nitrate and bECM solution. The valve of the separator funnel was slowly opened to allow the ammonium phosphate solution to drop over the calcium nitrate. The temperature of the calcium nitrate solution was maintained at 50°C and was kept under vigorous stirring. The solution slowly turns milky white in color indicating the formation of hydroxyapatite. The resulting milky white solution was then cooled to 4°C while being kept under constant stirring for another 24hrs at room temperature. After 24 hours the nano-hydroxyapatite precipitate is allowed to settle down in the beaker and the clear supernatant is removed carefully without disturbing the settled nHAP-bECM precipitates. The nHAP-bECM slurry at the bottom is then centrifuged to form a pellet and the supernatant is removed. The pellet is then mixed with deionized water and ultrasonicated for 10 minutes and then again centrifuged. This step is repeated 3-4 times to wash the nano-hydroxyapatite particles and remove all impurities. Finally the pellets are removed into a petridish and is kept for freezing at -20°C for 12 hours and were lyophilized in a freeze-dryer for 48 hr.

3.6.2 Characterization

The nano-hydroxyapatite and bone derived extracellular matrix composites were characterized by first X-ray diffraction by the same way described in section 3.3.2. The scanning range of 2θ was from 3° to 60°.

For Fourier Transform Infrared spectroscopic study the samples were suspended in deionized water with a concentration of 10mg/ml solution using ultrasonication. Then the FTIR was carried out as mentioned in section 3.3.2.

The morphology of the nHAP-bECM composites were analyzed using a Field Emission Scanning Electron Microscope as described in section 3.4.3.

3.7 DIP COATING OF bECM AND NANO-HYDROXYAPATITE-bECM COMPOSITE

Stainless steel sample coated with nHAP and sintered were were further coated with bECM and nHAP-bECM composite. For this dip coating method was used with the help of the fabricated dip coating device mentioned in section 3.1.3. For the bECM coating the nHAP coated sample was immersed in the bECM solution and then it was retracted from the solution at a speed of 4mm per minute. For the nHAP-bECM composite, sample S3 was suspended in in deionized water using ultra-sonication with a concentration of 50mg/ml. nHAP coated sample was then immersed in this solution and slowly retracted at the speed of 4mm per minute.

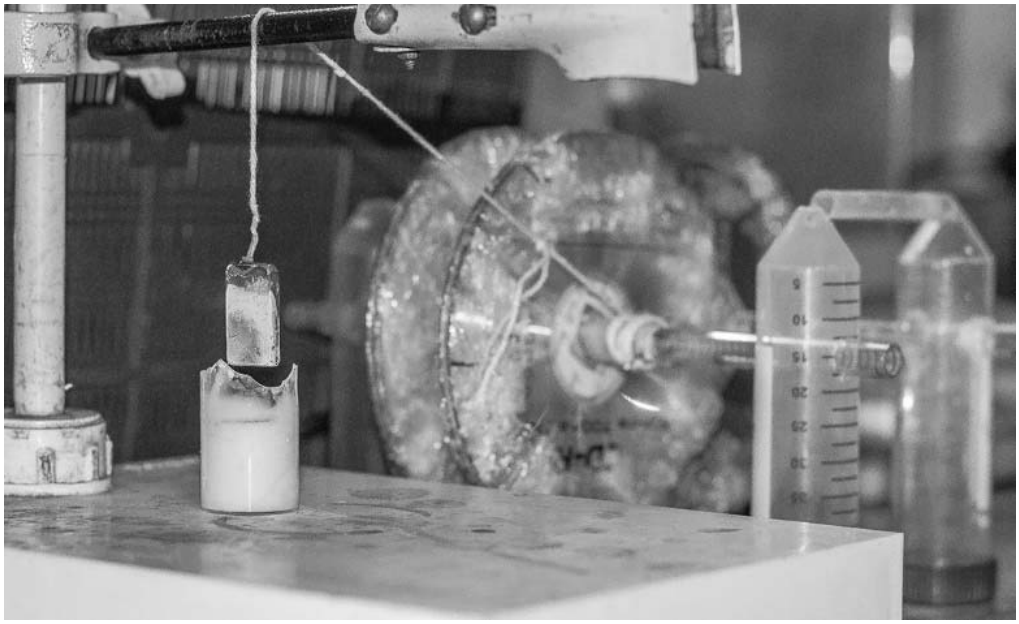

Figure 3.9: Dip coating of sample using the dip coating device

3.8 IN VITRO CELL PROLIFERATION ASSAYS

In vitro cytocompatibility of the nHAP-bECM composites and the steel samples coated with nHAP (control) as well as with bECM and nHAP-bECM composite was done using Adipose derived stem cells (ADSCs, HiMedia, Mumbai, India) as well as with MG63 cell lines (name of the company). These cells were maintained in DMEM (Dulbecco's modified eagle medium) medium supplemented with 10% Fetal Bovine Serum (FBS) as well as 1% antibiotics mixture of penicillin and streptomycin. In brief, the steel samples were at first kept for UV sterilization for 30 min., subsequently it was kept in a 70% ethanol solution for 30 min. and finally it was washed three times using PBS. After this both type of cells were seeded onto the steel samples at a concentration of $1x10^4$ cells/sample. The cells were then allowed to get adhered on the samples by keeping them for 48 h incubation in a CO_2 incubator maintained at 5% CO_2 level and 95% humidity at 37 ^{0}C. The complete media was supplemented time to time as per the requirements for maintaining the cell. After 48 h incubation the cell viability was calculated using the MTT assay method.

4 RESULTS AND DISCUSSIONS

4.1 SYNTHESIZED NANO-HYDROXYAPATITE CHARACTERIZATION AND ELECTROPHORETIC DEPOSITION STUDIES

4.1.1 Study of samples prepared by electrophoretic deposition

Figure 4.1 shows samples prepared using electrophoretic deposition at 100V and 200V with various concentration of nano-hydroxyapatite in propanol as electrolyte. It can be seen from these images that there are visible crack formations at higher concentration i.e. 10g/l and 20g/l. On further investigation of the samples deposited with lower concentration of nano-hydroxyapatite (5g/l) using SEM analysis it can be seen in Figure 4.2 that there are microscopic crack formations with more than 10µm in width and 100µm in length.

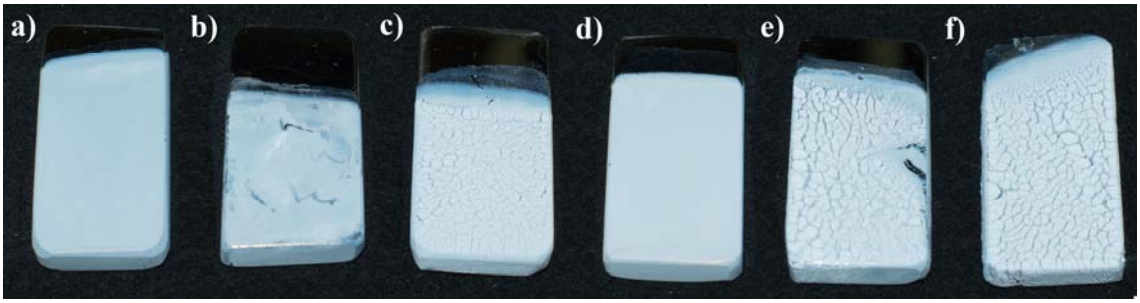

Figure 4.1: Picture of samples after EPD of nano-hydroxyapatite at 100V, a) 5g/l, b) 10g/l, c) 20g/l; and 200V, d) 5g/l, e) 10g/l, f) 20g/l

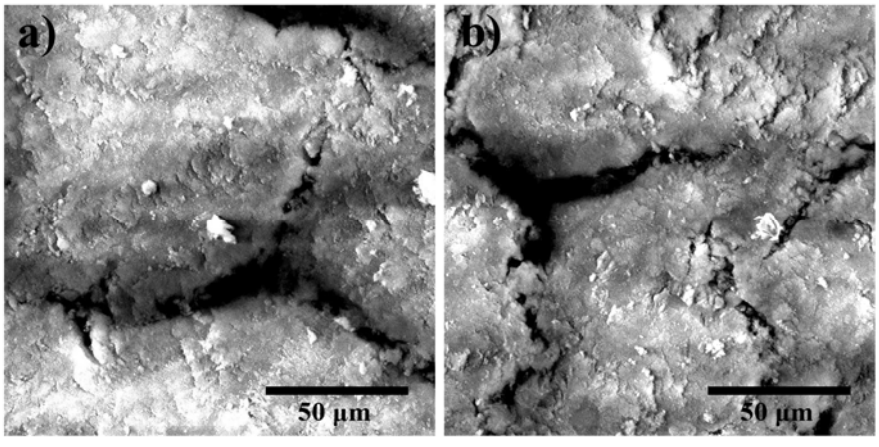

Figure 4.2: SEM images of sample 5g/l deposited at a) 100V and b) 200V

4.1.2 Kinetic study of electrophoretic deposition

Figure 4.3 shows the kinetic study of electrophoretic deposition of nano-hydroxyapatite on 316L stainless steel samples. It can be seen from the graph that the deposition was proportional to voltage applied and the concentration of nano-hydroxyapatite in the electrolyte solution. All the depositions rates are higher at first and then can be seen to slow down to a constant rate. This can be explained as nano-hydroxyapatite deposits and covers the surface of the steel sample creating a barrier between the positively charges nano-hydroxyapatite particles and the negatively charge steel sample surface, decreasing the rate to a lower constant value. Also in the graph it can be seen that there are several sudden slight increases in deposition rate in 20g/l nano-hydroxyapatite concentration electrolytes both at 100V and 200V. This can be explained as due to heavy deposition of nano-hydroxyapatite on the steel sample surface and then breaking off of some deposition back in to the electrolyte exposing the steel negatively charge free surface increasing the deposition rate.

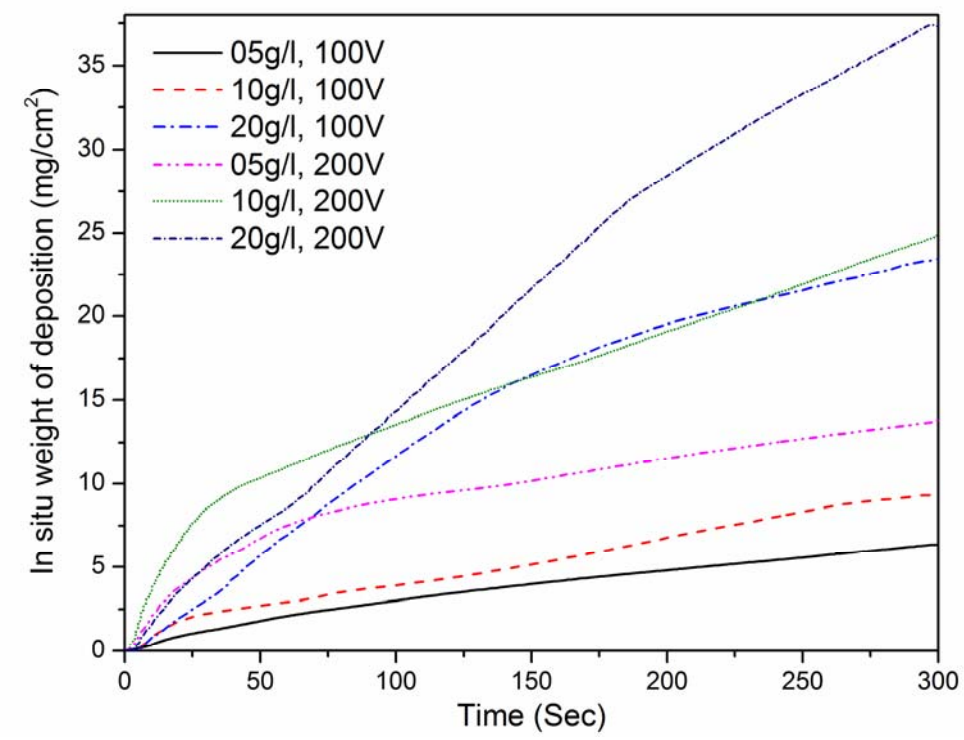

Figure 4.3: Deposition kinetics during EPD at 100V and 200V

4.1.3 Modified electrophoretic deposition procedure to reduce crack formation

Samples were electrophoretic deposited with a 10g/l nano-hydroxyapatite electrolyte solution at 30V for 2min, three times, with intervals between each deposition, in which sample were air dried. In this way any cracks developed from previous deposition was filled up by the consecutive deposition, as explained in Figure 4.4.

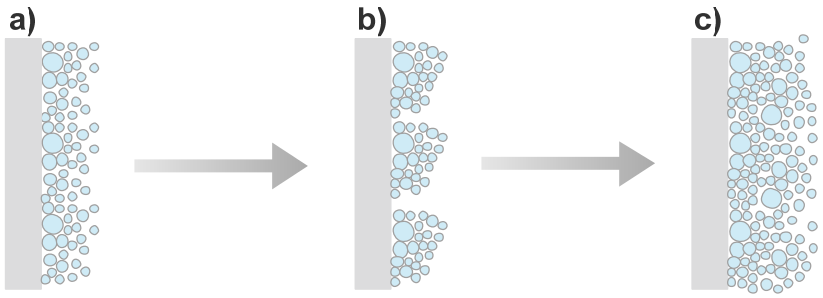

Figure 4.4: Deposited nano-hydroxyapatite after a) first coat, b) after drying and c) after second coat

4.1.4 Particle size analysis

Figure 4.5 show the size distribution of nano hydroxyapatite particles suspended in propanol solution. From the graph we can see there are two peaks corresponding to particle size of 233nm ± 90.16nm and 1297nm ± 512.3nm comprising 56.7% and 43.3% of all the particles respectively. The Z-average was calculated to be 321.2 d.nm.

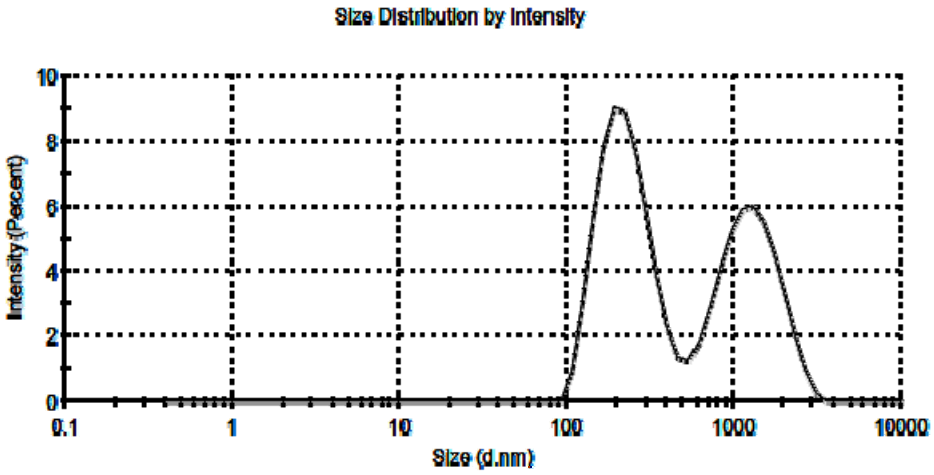

Figure 4.5: Size distribution curve of nano-hydroxyapatite

4.1.5 DSC-TG of nano-hydroxyapatite

Figure 4.6 show the DSC-TG plot of nano-hydroxyapatite deposited on 316L stainless steel. From the figure it has been observed that up to 100°C there is a decrease in mass and the DSC showing slight exothermic curve. This is due to the evaporation of water in the nano-hydroxyapatite powder. At 750-940°C we again see a decrease DSC curve implying an exothermic reaction. This is can be due to sintering of the nano-hydroxyapatite releasing energy from the bond formation between the hydroxyapatite molecules. At around 975° we can see rapid decrease in mass, probably due to decomposition of nano-hydroxyapatite.

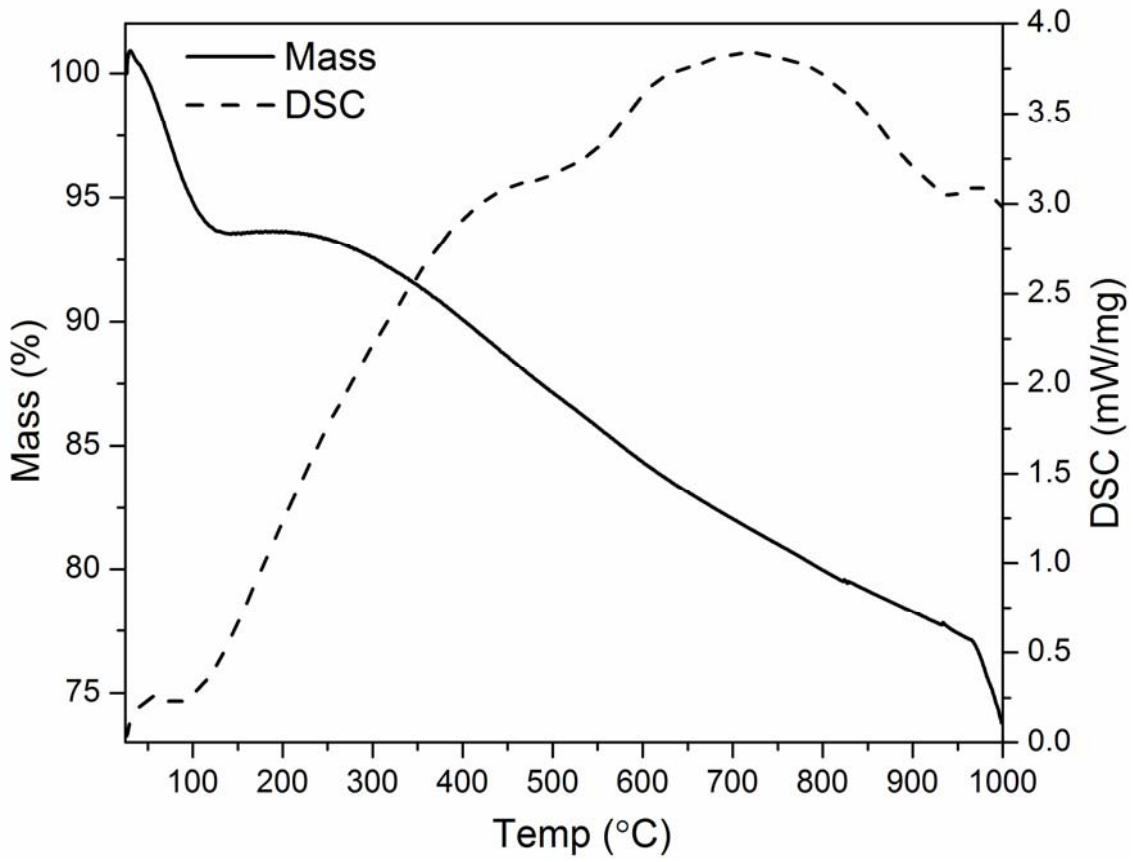

Figure 4.6: DSC-TG study of nano-hydroxyapatite powder deposited over 316L stainless steel samples

4.1.6 XRD of nano-hydroxyapatite before and after sintering

Figure 4.7 shows the XRD of nano-hydroxyapatite before and after sintering at 900°C in argon atmosphere in a tube furnace. The XRD pattern and peak was matched to that of standard JCPDS file no. (82-1943), confirming hydroxyapatite (synthesized).

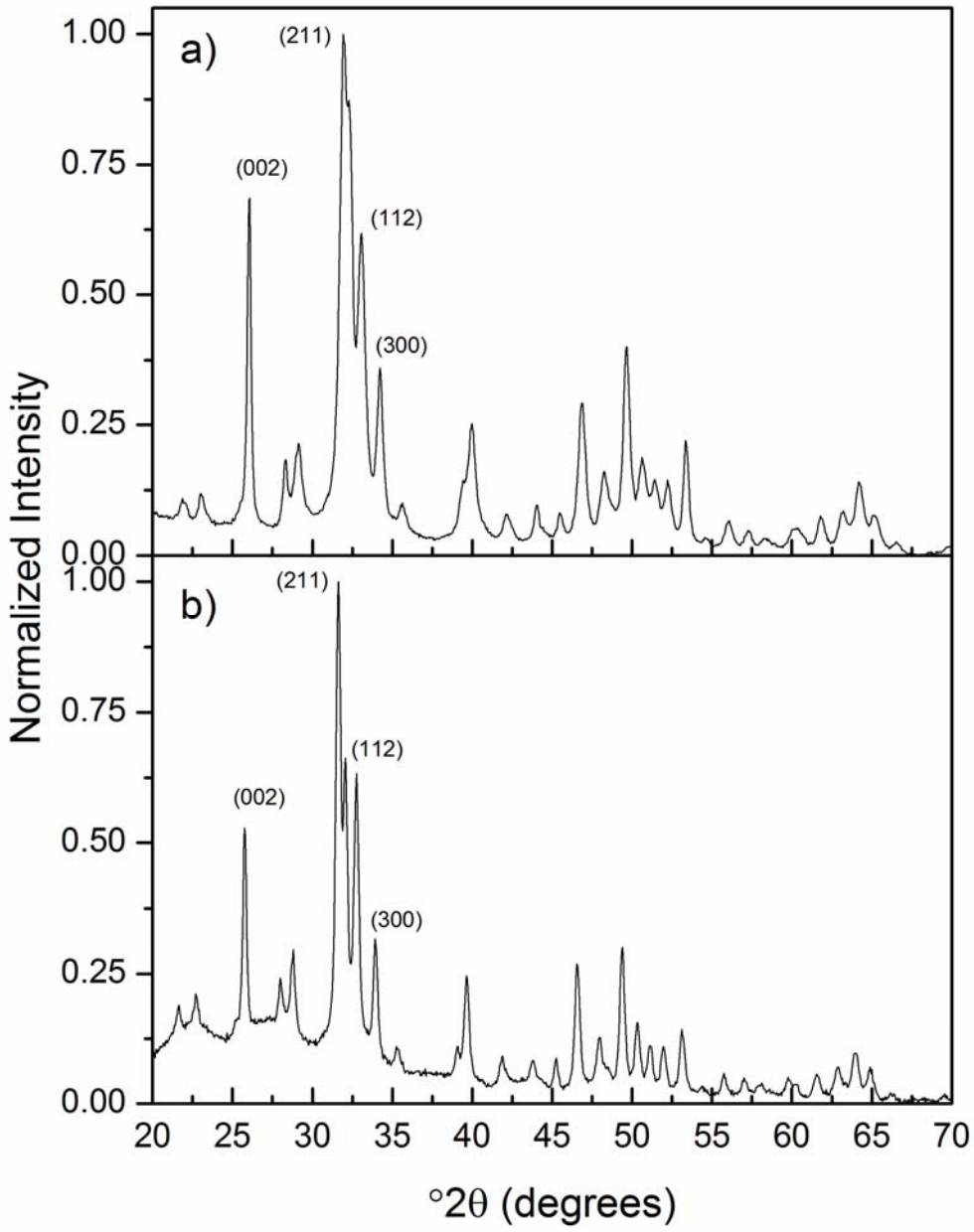

Figure 4.7: XRD of nano-hydroxyapatite a) before and b) after sintering

4.1.6.1 Crystalline Size

Crystalline size was calculated using the following Debye–Scherrer equation. [20]

$$X_S = \frac{0.9\lambda}{\beta cos\theta}$$

Where X_S is the crystalline size, λ is the wavelength of X-ray beam, β is the Full Width at Half Maximum (FWHM) of the peak at the maximum intensity and θ is the peak diffraction angle. From this the average[1] crystalline size was found to increase from 25.6 nm to 28.4 nm after sintering.

Table 4.1: Crystalline size of selected planes of nano-hydroxyapatite before sintering

Plane	Angle of diffraction (°2θ)	FWHM	Crystalline Size X_S (nm)	Specific surface area (m^2/g)
0 0 2	26.0	0.24	33.9	55.9
2 1 1	31.9	0.42	19.6	96.5
1 1 2	32.3	0.3	27.6	68.9
3 0 0	33.0	0.48	17.2	110.0

Table 4.2: Crystalline size of selected planes of nano-hydroxyapatite after sintering

Plane	Angle of diffraction (°2θ)	FWHM	Crystalline Size X_S (nm)	Specific surface area (m^2/g)
0 0 2	25.7	0.24	33.9	55.9
2 1 1	31.6	0.3	27.5	69.0
1 1 2	32.0	0.24	34.4	55.2
3 0 0	32.7	0.3	27.5	68.8

[1] Average crystalline size was calculated considering all the peaks in the XRD curve.

4.1.6.2 Degree of Crystallization

The degree of crystallinity (X_C) was calculated using the following equation. [21]

$$X_C = 1 - \left(V_{112/300}/I_{300}\right)$$

Where, $V_{112/300}$ is the intensity of the valley between the diffraction peak (112) and (300) of nano-hydroxyapatite and I_{300} is the intensity of the diffraction peak (300). After sintering the degree of crystallization was found to increase from 71.6% to 90.4%.

4.1.6.3 Specific surface area of crystals before sintering

Specific surface area of the HAP determined by the formula [22]

$$S = 6 \times 10^3/d\rho \qquad (d=3.16\ g/cm^3)$$

Where ρ is the crystallite size (nm) and d is the theoretical density of hydroxyapatite. Average[2] surface area was found to decrease from 83.46 m^2/g to 71.42 m^2/g after sintering.

[2] Average surface area was calculated considering all the peaks in the XRD curve.

4.1.7 FTIR

Figure 4.8 shows the FTIR of the nano hydroxyapatite before and after the sintering at 900°C in argon atmosphere. Analysis of the FTIR peaks showed the presence of OH group (3613 cm^{-1}), CO_3 group (1463 cm^{-1}) and PO_4 group (1041 cm^{-1} and 570 cm^{-1}). Apart from the peak intensity change, there was no significant difference before and after the sintering process.

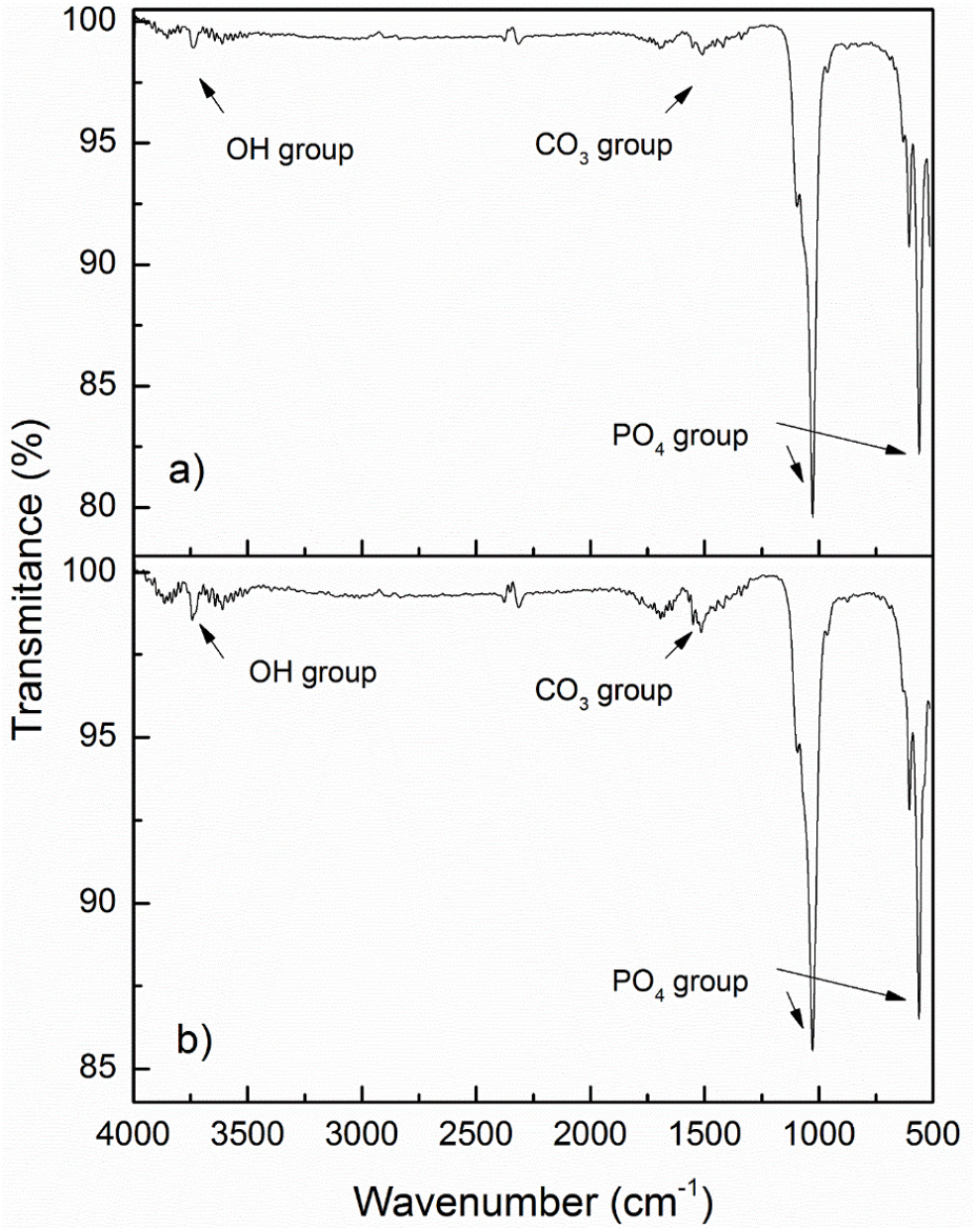

Figure 4.8: FTIR of nano-hydroxyapatite a) before and b) after sintering

4.1.8 FE-SEM analysis

From FE-SEM images (Figure 4.11) nano-hydroxyapatite were found to have needle shaped particles with diameter of average 39nm and length of 340nm. After sintering the crystals fused together to form average 43nm width grain size. There were very few cracks less than a micrometer width. Focusing inside the cracks showed nano-hydroxyapatite coat of previous layer, hence the metal surface was not exposed.

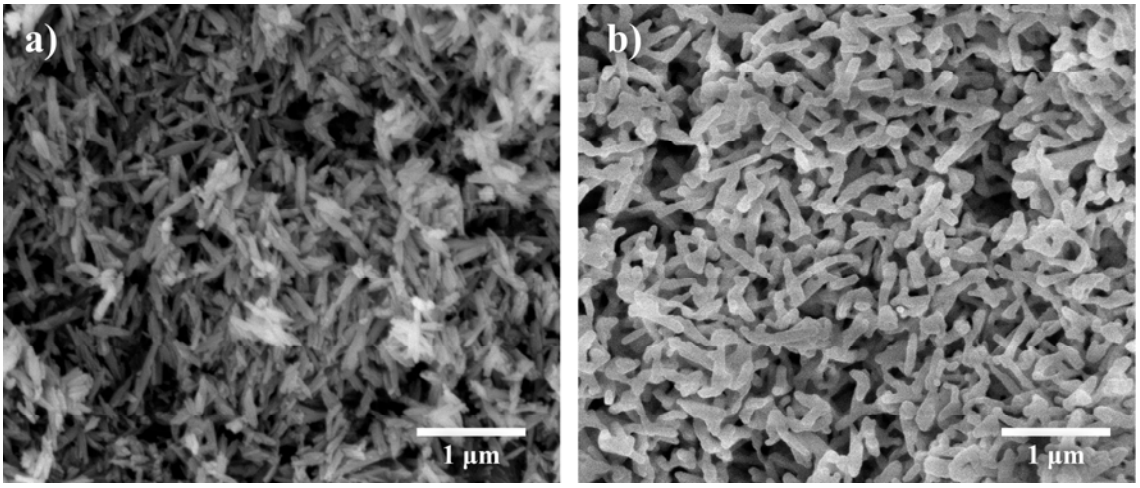

Figure 4.9: FE-SEM of samples a) before and b) after sintering at 900°C

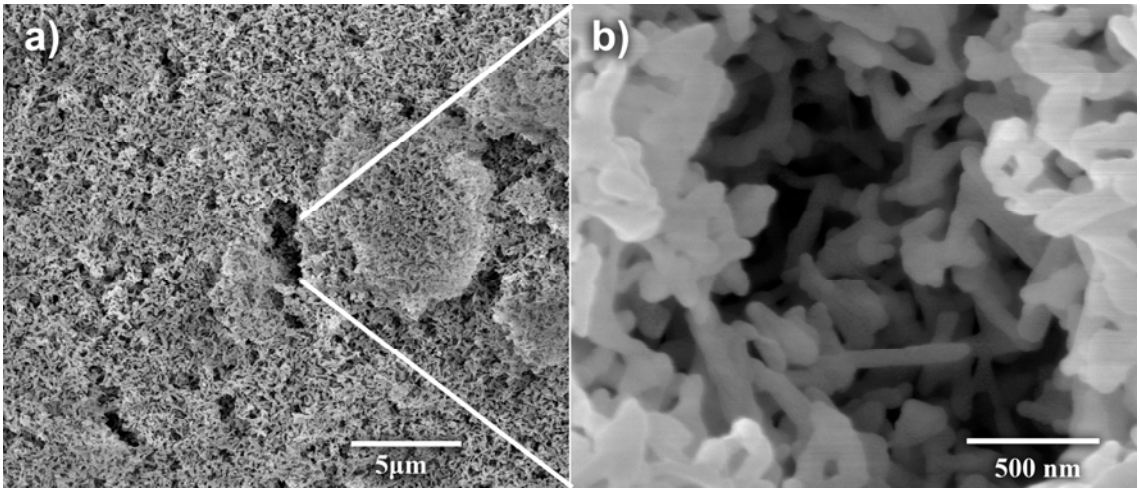

Figure 4.10: FE-SEM of deposited nano-hydroxyapatite at 30V interval EPD showing a) micro crack and its b) magnification

4.2 BONE DERIVED ECM (BECM) CHARACTERIZATION AND ANALYSIS

4.2.1 Protein estimation using Lowry's Method

Figure 4.11 shows the standard curve of Lowry's estimation method that was plotted using BSA as standard protein solution. The concentration of the resulting solution of extracted bECM was found to be 12.23mg/ml.

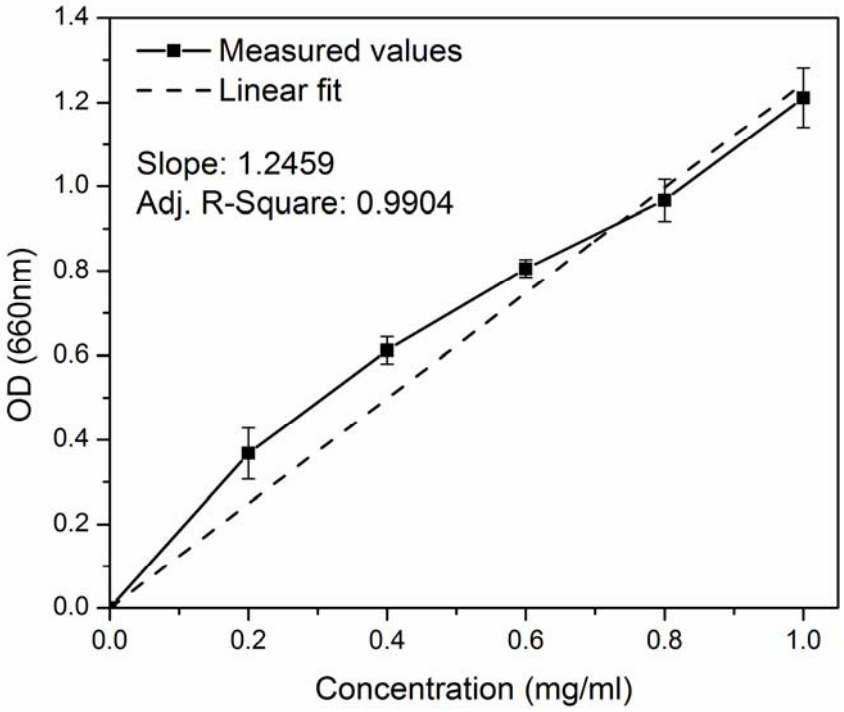

Figure 4.11: Lowry's protein estimation standard curve

4.2.2 Collagen Estimation

From the hydroxyproline assay, the collagen content bovine derive extracellular matrix was found to be 0.82 ± .029 mg per mg of its lyophilized powder.

4.2.3 SDS PAGE

Figure 4.12 show the SDS PAGE of the bovine derived extracellular matrix. We can see four major bands in the lane of bovine derived extracellular matrix. There are two bands between the 205 and 97.4 kDa protein markers. As we know collagen I comprises 90% ofThese two can be said to correspond to Collagen I αI and Collagen I αII which are of size of 139kDa and 129kDa respectively. Further there is a dark band and light band is visible between 43kDa and 29kDa which can be due to presence of Osteopontin which is of size 42kDa and 33kDa is nascent form. Osteopontin is found in abundance in bone matrix among the non-collagenous proteins constituting 1-2% of total bone proteins. Other than that there is a wide dark band at 20.1kDa protein marker. This comprises of all the proteins less than 20.1kDa that did not resolve. It may contain proteins like Osteocalcin which is of 7kDa.

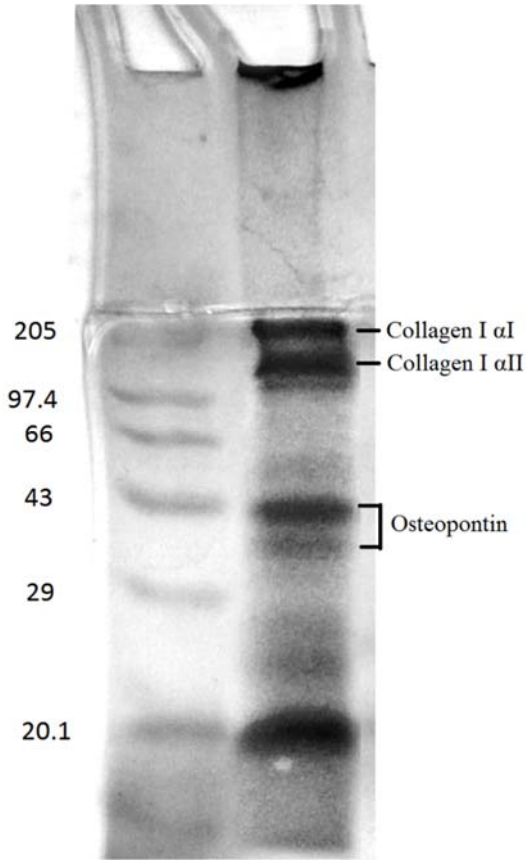

Figure 4.12: SDS PAGE of bovine derive extracellular matrix

4.3 nHAP-bECM COMPOSITE

4.3.1 FTIR of samples in solution form

Figure 4.13 shows the FTIR of the nHAP-bECM composites in solution form. In sample S2, S3, S4, S5 and bECM Amide I and Amide II peaks can be seen at 1680-1640cm^{-1} and 1550-1520cm^{-1} respectively with increasing intensity showing the increase of protein content in the composites. Presence of phosphate group is seen at 1030cm^{-1} in all the composites confirming the presence of hydroxyapatite.

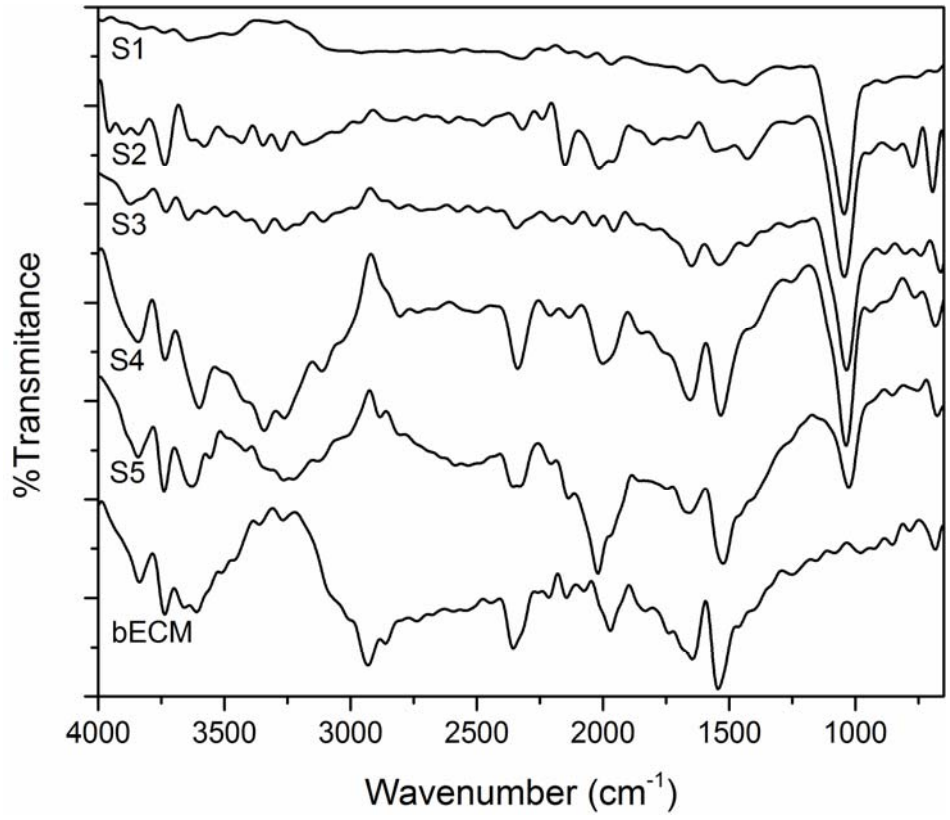

Figure 4.13 FTIR of sample in solution form

4.3.2 Crystallinity of samples using XRD and FTIR

Crystallinity index of the samples were calculated from the XRD and FTIR (Figure 4.14 and Figure 4.15) using the methods described in previous studies [23] [24]. Following equations were used to calculate the crystalline size and degree of crystallinity. Table 4.3 shows the comparison of the samples. With increasing concentration the degree of crystallinity increased till Sample S3 and then a decrease in crystallinity is observed.

Crystalline Size:

$$X_S = \frac{0.9\lambda}{\beta cos\theta}$$

(Calculated considering plane (211))

Crystallinity Index:

$$CI_{XRD} = \frac{I_{112} + I_{300} + I_{202}}{I_{211}}$$

$$CI_{FTIR} = \frac{A_{565} + A_{605}}{A_{595}}$$

Table 4.3 Crystallinity index of nano-hydroxyapatite-bECM composite samples

Sample	X_S (nm)	CI_{XRD}	CI_{FTIR}
S1 (HAP)	11.5	0.043	2.45
S2 (HAP + 0.5 bECM)	15.3	0.052	2.53
S3 (HAP + 1.0 bECM)	17.2	0.145	3.62
S4 (HAP + 1.5 bECM)	19.7	0.037	3.40
S5 (HAP + 2.0 bECM)	15.3	0.020	3.10

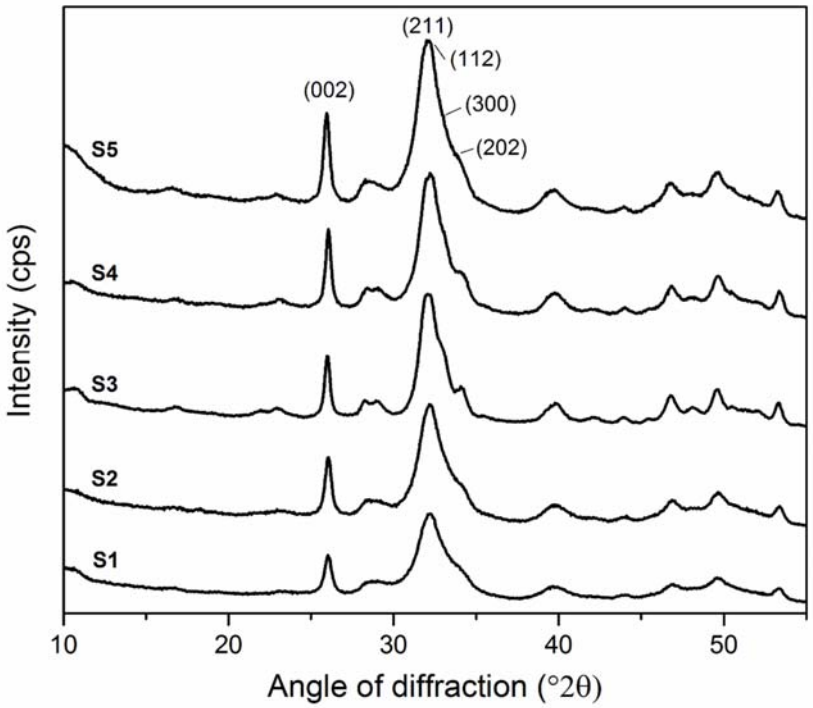

Figure 4.14: XRD of nano-hydroxyapatite-bECM composite samples (S2-S5) and HAP as control (S1)

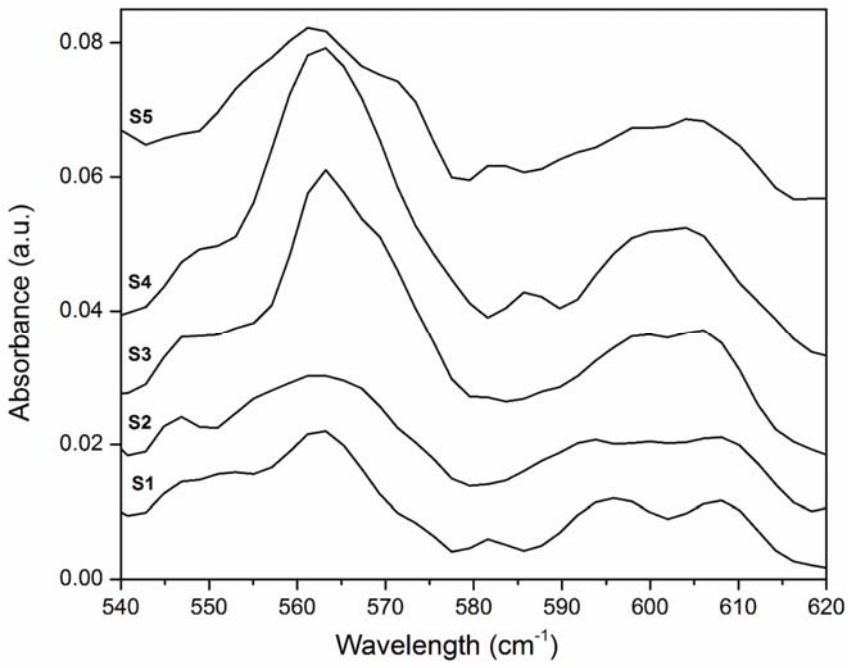

Figure 4.15: FTIR of nano-hydroxyapatite-bECM composite samples (S2-S5) and HAP as control (S1)

4.3.3 DSC-TGA

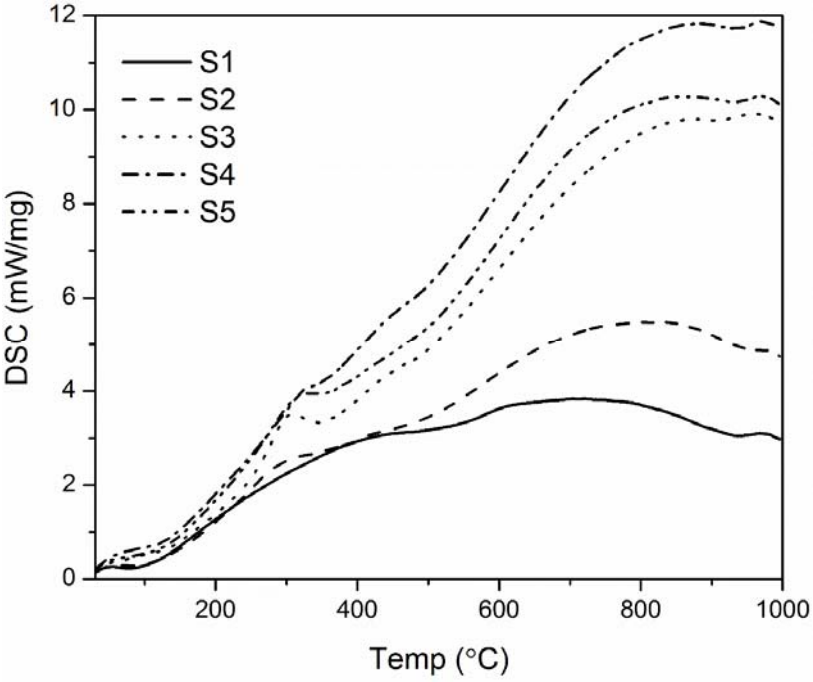

Figure 4.16: DSC of nano-hydroxyapatite-bECM composite samples (S2-S5) and HAP as control (S1)

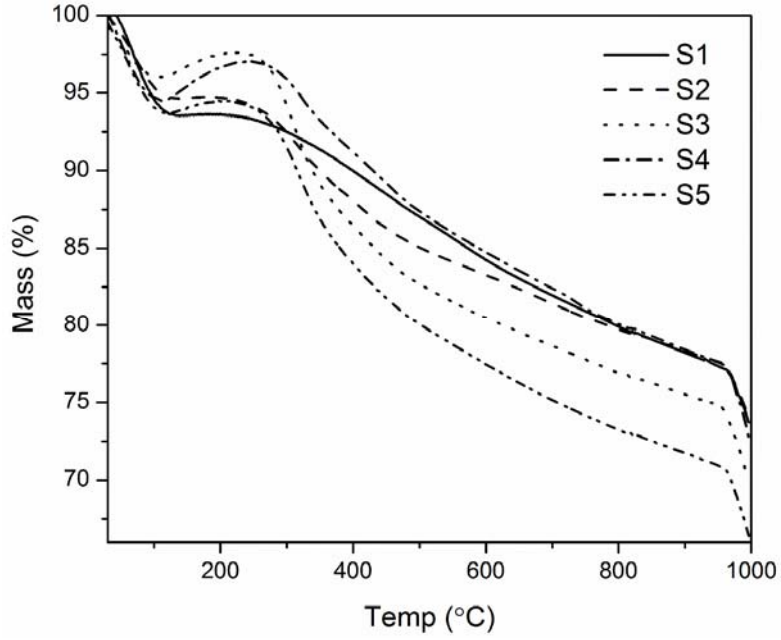

Figure 4.17: TGA of nano-hydroxyapatite-bECM composite samples (S2-S5) and HAP as control (S1)

4.3.4 FE-SEM

Figure 4.18 shows the FESEM of nHAP and bECM samples taken at 100,000x magnification. We can see sample S1 showing globular and feathery particles. Sample S2 and S4 shows feathery structures. Sample S3 shows compact globular structures. Sample S5 with highest concentration of bECM is showing fibrous structures. Figure 4.17 f) is the FESEM of bECM which shows flakey structures of lyophilized bECM.

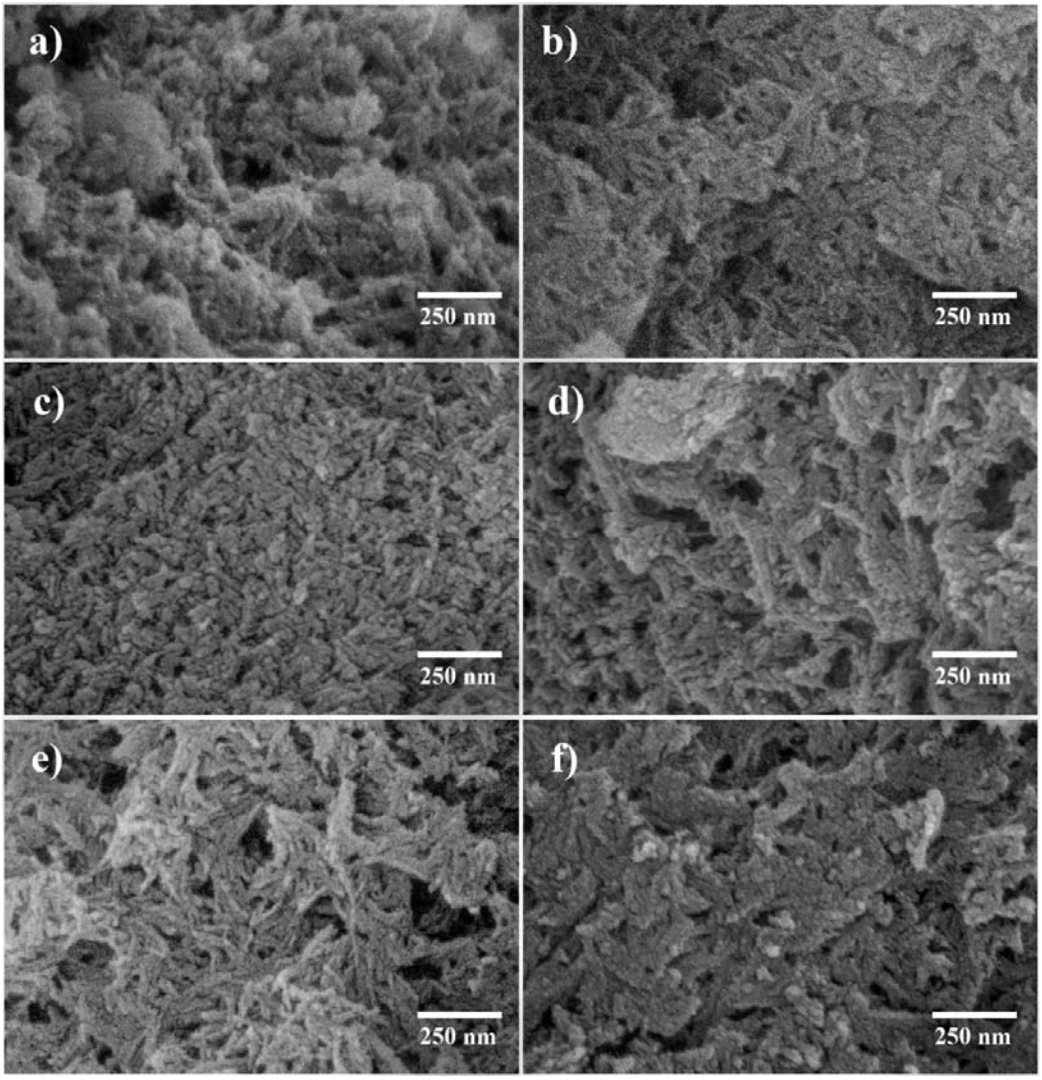

Figure 4.18: FESEM of samples a) S1 (HAP), b) S2 (HAP + 0.5 bECM), c) S3 (HAP + 1.0 bECM), d) S4 (HAP + 1.5 bECM), e) S5 (HAP + 2.0 bECM), f) bECM

4.4 IN-VITRO CELL PROLIFERATION AND DIFFERENTIATION ASSAY

Figure 4.19 show the MTT cell proliferation assay of the nHAP and bECM composites. The MTT was carried out for adipose derive stem cells. From the graph it can be seen that sample S1 and S2 showed slight increase from the control but not statistically significant. Whereas sample S3, S4 and S5 showed significant increase in cell proliferation from the control and S1. Though they were not statistically significant among themselves.

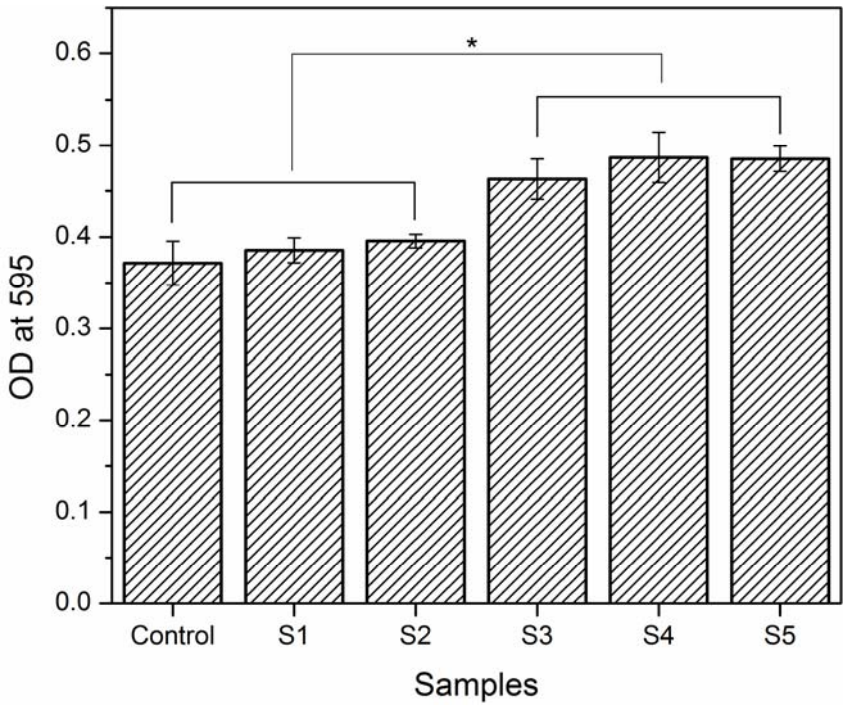

Figure 4.19: MTT cell proliferation assay of samples

4.5 CONCLUSION

So from this study it can be said that the nano-hydroxyapatite and bone derived extracellular matrix increased the cell proliferation at higher concentration of extracellular matrix in the composite. So this composite coating should increase the bioactivity and the osteointegration of the implants. But before the use as implant of these nano hydroxyapatite and bone derived extracellular matrix composite coating on 316L stainless steel various further tests are required. Tests like corrosion resistivity to check if the implants can be used for long time, immuno tests to see if the xenogenic extracellular matrix causes any immune reaction, in vivo testing using animal models to check the osteointegration of implants etc.

REFERENCES

[1] D. Bociaga, "Praca doktorska," *Politechnika Lodzka,* 2007.

[2] J. J. Jacobs, J. L. Gilbert and R. M. Urban, "Current Concepts Review-Corrosion of Metal Orthopaedic Implants*," *The Journal of Bone \& Joint Surgery,* vol. 80, no. 2, pp. 268-82, 1998.

[3] T. Hanawa, "Metal ion release from metal implants," *Materials Science and Engineering: C,* vol. 24, no. 6, pp. 745-752, 2004.

[4] Y. Ikada, "Surface modification of polymers for medical applications," *Biomaterials,* vol. 15, no. 10, pp. 725-736, 1994.

[5] K. De Groot, R. Geesink, C. Klein and P. Serekian, "Plasma sprayed coatings of hydroxylapatite," *Journal of biomedical materials research,* vol. 21, no. 12, pp. 1375-1381, 1987.

[6] C. Ossa, S. Rogero and A. Tschiptschin, "Cytotoxicity study of plasma-sprayed hydroxyapatite coating on high nitrogen austenitic stainless steels," *Journal of Materials Science: Materials in Medicine,* vol. 17, no. 11, pp. 1095-1100, 2006.

[7] D.-M. Liu, Q. Yang and T. Troczynski, "Sol--gel hydroxyapatite coatings on stainless steel substrates," *Biomaterials,* vol. 23, no. 3, pp. 691-698, 2002.

[8] V. K. Balla, M. Das, S. Bose, G. J. Ram and I. Manna, "Laser surface modification of 316L stainless steel with bioactive hydroxyapatite," *Materials Science and Engineering: C,* vol. 33, no. 8, pp. 4594-4598, 2013.

[9] I. Zhitomirsky and L. Gal-Or, "Electrophoretic deposition of hydroxyapatite," *Journal of Materials Science: Materials in Medicine,* vol. 8, no. 4, pp. 213-219, 1997.

[10] J.-H. Park, D.-Y. Lee, K.-T. Oh, Y.-K. Lee, K.-M. Kim and K.-N. Kim, "Bioactivity of calcium phosphate coatings prepared by electrodeposition in a modified simulated body fluid," *Materials letters,* vol. 60, no. 21, pp. 2573-2577, 2006.

[11] S. F. Badylak, "The extracellular matrix as a biologic scaffold material," *Biomaterials,* vol. 28, no. 25, pp. 3587-3593, 2007.

[12] A. S. Greenwald, S. D. Boden, V. M. Goldberg, Y. Khan, C. T. Laurencin, R. N. Rosier and others, "Bone-graft substitutes: facts, fictions, and applications," *The Journal of Bone \& Joint Surgery,* vol. 83, no. 2 suppl 2, pp. S98--103, 2001.

[13] B. Peterson, P. G. Whang, R. Iglesias, J. C. Wang and J. R. Lieberman, "Osteoinductivity of commercially available demineralized bone matrix," *The Journal of Bone \& Joint Surgery,* vol. 86, no. 10, pp. 2243-2250, 2004.

[14] E. Bouyer, F. Gitzhofer and M. Boulos, "Morphological study of hydroxyapatite nanocrystal suspension," *Journal of Materials Science: Materials in Medicine,* vol. 11, no. 8, pp. 523-531, 2000.

[15] L. Yubao, C. Klein, J. de Wijn, J. Wolke and K. de Groot, "Morphology and phase structure of nanograde boneapatite-like rodshaped crystals," *Bioceramics. Philadelphia, USA: Butterworth-Heinemann,* pp. 173-8, 1993.

[16] A. C. Tas, "Synthesis of biomimetic Ca-hydroxyapatite powders at 37 C in synthetic body fluids," *Biomaterials,* vol. 21, no. 14, pp. 1429-1438, 2000.

[17] C. Ohtsuki, T. Kokubo and T. Yamamuro, "Mechanism of apatite formation on CaO SiO 2 P 2 O 5 glasses in a simulated body fluid," *Journal of Non-Crystalline Solids,* vol. 143, pp. 84-92, 1992.

[18] M. Ferraz, F. Monteiro and C. Manuel, "Hydroxyapatite nanoparticles: a review of preparation methodologies," *Journal of Applied Biomaterials and Biomechanics,* vol. 2, no. 2, pp. 74-80, 2004.

[19] E. Gruskin, B. A. Doll, F. W. Futrell, J. P. Schmitz and J. O. Hollinger, "Demineralized bone matrix in bone repair: history and use," *Advanced drug delivery reviews,* vol. 64, no. 12, pp. 1063-1077, 2012.

[20] S. Danilchenko, O. Kukharenko, C. Moseke, I. Y. Protsenko, L. Sukhodub and B. Sulkio-Cleff, "Determination of the bone mineral crystallite size and lattice strain from

diffraction line broadening," *Crystal Research and Technology,* vol. 37, no. 11, pp. 1234-1240, 2002.

[21] Y. Pang and X. Bao, "Influence of temperature, ripening time and calcination on the morphology and crystallinity of hydroxyapatite nanoparticles," *Journal of the European Ceramic Society,* vol. 23, no. 10, pp. 1697-1704, 2003.

[22] M. Bhagwat, P. Shah and V. Ramaswamy, "Synthesis of nanocrystalline SnO 2 powder by amorphous citrate route," *Materials Letters,* vol. 57, no. 9, pp. 1604-1611, 2003.

[23] A. Person, H. Bocherens, J.-F. Sali{\`e}ge, F. Paris, V. Zeitoun and M. G{\'e}rard, "Early diagenetic evolution of bone phosphate: an X-ray diffractometry analysis," *Journal of Archaeological Science,* vol. 22, no. 2, pp. 211-221, 1995.

[24] J. Reyes-Gasga, E. L. Martierardnez-Pineiro, G. Rodriguez-Alvarez, G. E. Tiznado-Orozco, R. Garcia-Garcia and E. F. Brees, "XRD and FTIR crystallinity indices in sound human tooth enamel and synthetic hydroxyapatite," *Materials Science and Engineering: C,* vol. 33, no. 8, pp. 4568-4574, 2013.

[25] M. Sawkins, W. Bowen, P. Dhadda, H. Markides, L. Sidney, A. Taylor, F. Rose, S. Badylak, K. Shakesheff and L. White, "Hydrogels derived from demineralized and decellularized bone extracellular matrix," *Acta biomaterialia,* vol. 9, no. 8, pp. 7865-7873, 2013.